Chapter 6

Recombination Lines from the Galactic HII complex W3

6.1 Introduction

In this chapter, we present a study of another type of CII region from which carbon recombination lines are detected at relatively high frequencies ($\nu > 1$ GHz). These regions occur adjacent to and surrounding some of the bright HII regions, which happen to be ionization bounded *i.e.* there is neutral matter surrounding the HII region for which there are not enough photons with energies > 13.6 eV to fully ionize it. However, hydrogen can be partially ionized in a small region surrounding the HII region, by the few energetic photons that escape from the fully ionized region. Such regions form the partially ionized medium (PIM or H^o). The current picture for the relative location of the HII, H^o (partially ionized medium where hydrogen is fractionally ionized) and CII region is shown in Fig 6.1 (from Roelfsema & Goss 1992). The stellar photons with energies ≥ 11.4 eV which escape from the HII region, ionize the carbon and other heavier elements in the surrounding neutral hydrogen regions giving rise to CII zones (Fig 6.1). The CII region associated with the HII region W3A is an example of this type and this chapter discusses some observations of this region. Furthermore, molecular hydrogen can be dissociated (dissociation energy ~ 4.5 eV) and a region of neutral HI can also exist. This neutral hydrogen gas near HII regions forms the high-excitation photodissociation region (PDR) which as defined by Tielens & Hollenbach (1985) is a " region where FUV radiation ($6 - 13.6$ eV) dominates the heating and/or some important aspect of the chemistry". .Such regions consist of both atomic and molecular gas. Observations of HII regions, with associated PIM & PDR, at low frequencies (~ 1 GHz) reveal three to four types of recombination lines. These are the broad hydrogen line from the HII region and the narrow ($\Delta V < 10$ kms^{-1}) hydrogen,

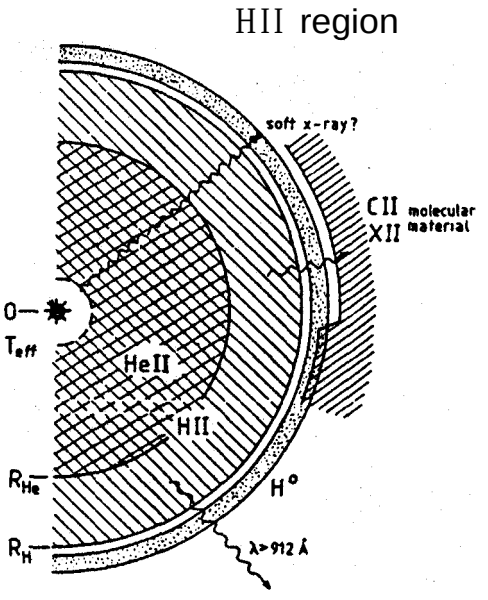

Figure 6.1 (a) **Schematic representation of a CII region near a HII region. X represents the elements other than carbon, hydrogen and helium. H° represents the partially-ionized medium (taken from Roelfsema & Goss 1992).**

carbon and possibly sulphur lines from the PIM or PDR. The Galactic HII region W3 is a good example which exhibits such lines. We refer to the region in which the narrow hydrogen lines arise as the H^o region and the region in which carbon lines form as the CII region.

W3(core) is a complex of HII regions and molecular clouds at a distance of 2.4 kpc in the Perseus spiral arm. It consists of HII regions in various evolutionary stages as judged from their angular dimensions. W3A is the largest and the most evolved component which is widely studied in continuum and spectral lines over a wide range of the electromagnetic spectrum.

Radio recombination lines of hydrogen, helium, carbon and sulphur have been observed from W3A. Pankonin *et.al.* (1977) detected a hydrogen line (H166α) composed of two components with widths of 28 and 7 kms^{-1} in their single-dish observations. van Gorkom (1980) also found the hydrogen line detected in her interferometric observations to consist of two components. However the widths of the two components were $\sim$ 70 kms^{-1} and $\sim$ 7 kms^{-1}. The broad component was very weak, and could be seen only in the profile integrated over the entire continuum source W3A. A similar result was obtained by Roelfsema (1987). Thus, although the width of the narrow hydrogen component which is strong and appeared as a sharp feature above the broad pedestal, matched in all these observations, the width of the broad component is discrepant in

different observations. High-sensitivity observations are therefore required to clearly distinguish the broad component and to separate the narrow component from the combined profile.

That a CII region is associated with the HII region in W3A has been demonstrated by many observations including that of Pankonin *et.al.* (1977) who detected carbon recombination lines over a range of frequencies from W3. The lines could be explained if the emitting region was at a temperature $\sim$ 150 K and had an electron density of $\sim 25\ \mathrm{cm}^{-3}$. The main mechanism for the observed line being stimulated emission in a region in front of the bright HII region due to the strong background continuum. The carbon line emission from W3A near 1.4 GHz has been mapped by Roelfsema *et.al.* (1987) with a resolution of $\sim$ 14" and they find the emission to be confined to the location of the continuum source, thus confirming the importance of stimulated emission. However, the line emission displays structure which is different from that of the continuum and the authors interpret it as being due to variations in the physical properties of the emitting gas. If the distribution of the carbon line emission can be compared with the narrow hydrogen line emission then interesting questions regarding the association of CII & H^{o} regions can be addressed. Onello & Phillips (1995) have found a strong correlation between the normalized intensities of the carbon and narrow hydrogen lines in a comparative study of six HII regions. They conclude that the excitation conditions in the regions from which the narrow hydrogen lines and carbon lines arise are the same. The spatial distributions of both the recombination lines should be similar if they arise in coexistent media. The main goal of this study is to test this similarity using high-sensitivity and high-resolution observation of carbon and hydrogen recombination lines at a frequency near 1.4 GHz from the source W3A.

We present in this chapter, a comparative study of the emission in narrow hydrogen and carbon lines over the face of W3A and discuss the probable physical properties of the partially ionized medium. The continuum emission from W3A and broad hydrogen recombination line together with other available data are used to obtain constraints on the electron temperature, density and clumpiness in the hot HII region.

6.2 Observations & Results

W3 was observed in the 20 cm band using the Very Large Array (VLA) in its B-configuration for a total of 11 hours spread over three observing sessions in 1993 and 1995. The details of the observations are listed in Table 6.1. The data were reduced using the AIPS software package developed by NRAO.

Table **6.1 Observational Details**

1	Transitions observed	H168α, C168α
2	Rest Frequencies	1374.6 MHz & 1375.3 MHz
3	Central velocity of observation	-60 kms^{-1}
4	Central frequency of observation	1374.8 MHz
5	Bandwidth	1.562 MHz (340 kms^{-1})
6	Number of channels	127
7	Spectral resolution	12.2 kHz (2.7 kms^{-1})
8	Observing dates & duration	20 March 1993 - 5h 09 April 1993 - 3h 22 Novem 1995 - 3h
9	VLA Array Configuration	B
10	Primary beam	30'
11	Synthesized beam (naturally weighted)	5.7" x 5.5"
12	Primary flux density calibrator Flux density of 0134+329	0134+329 16.5 Jy
13	Phase calibrator	0212+735
14	Bandpass calibrator	0134+329
15	Phase Centre : α(1950) δ(1950)	 02 21 49 61 52 40
16	rms noise in continuum image	2 mJy/beam
17	rms noise in the line image	1 mJy/beam

The visibility data from different observing sessions were calibrated separately and then combined to get the final data set. The continuum emission was subtracted from the line data set by removing a linear baseline determined from the channels devoid of line emission. After applying natural weighting to the visibilities, continuum and line images were made. The continuum image shown in Fig 6.2 was made after deconvolving the dirty image using the "CLEAN" algorithm. Since the continuum source is bright, self-calibration was used to further correct any residual phase errors in both the line & continuum visibilities. The rms noise in the self-calibrated continuum image is 2 mJy/beam and the angular resolution is 5.7" x 5.5". A line cube (512 x 512 x 127) was constructed by fourier transforming the continuum-subtracted and self-calibrated visibility data of all the channels. Only those channels which displayed significant line emission were "cleaned" to remove the sidelobe response. The rms noise in the channel images is $\sim$ 1 mJy/beam. Since the line emission appeared extended, the line images

were smoothed to 10" x 10" resolution to increase the signal-to-noise ratio. The rms noise on these images is $\sim$ 1.8 mJy/beam.

The 20 cm continuum map at a spatial resolution 5.7" x 5.5" of the W3 complex of HII regions in the Perseus arm is shown in Fig 6.2. The W3 complex consists of eight HII regions A to H as shown in the Fig. W3A, the largest HII region is resolved and it displays a broken shell morphology with the shell opening to the south. W3C, W3E, W3F and W3G are unresolved. W3B is a bright HII region. W3D and W3H are low-brightness extended HII regions presumably in relatively advanced stages of evolution.

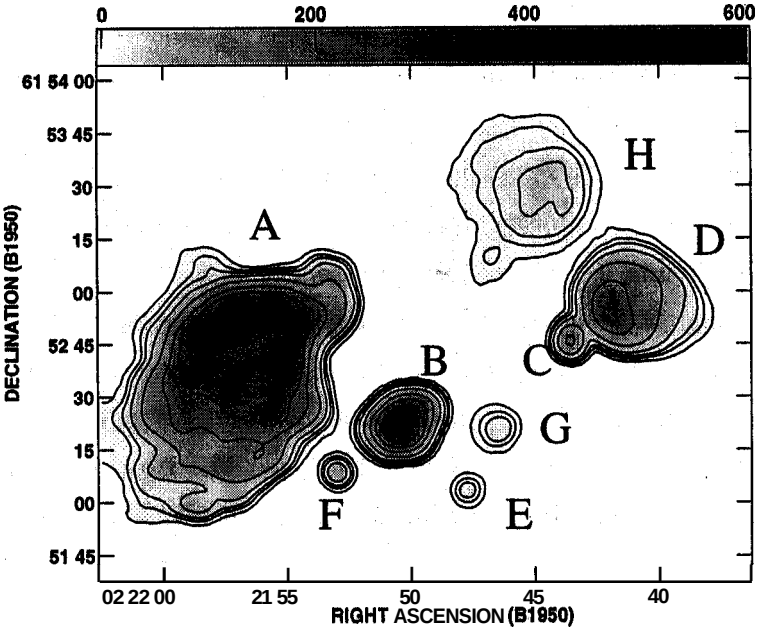

Figure 6.2 Continuum image of W3(core) near 20 cm at an angular resolution of 5.7″ x 5.5″ and P.A. = −89°. A to H are the 8 HII regions in the core region of W3. The grey scale flux ranges from 0 to 0.6 Jy/beam. The contours levels are 1,2,3,5,10,20,30,40,50 in units of 8.5 mJy/beam. The continuum flux density of W3A near 20 cm is 17 Jy.

The line spectra integrated over the different continuum sources are shown in Fig 6.3 (a) to (d). H168α line emission is detected from W3A, W3B, W3C+W3D and W3H whereas only W3A clearly shows the presence of a C168α line. Gaussians were fitted to the observed profile and the best fit parameters are listed in Table 6.2. The

Table 6.2 **Results of the Gaussian fits to 168α line profiles from various HII regions in the W3 complex.**

No.	Source	Line	Peak Line S_L (Jy/beam)	V_{lsr} kms^{-1}	ΔV(FWHM) kms^{-1}
1	W3A	H168α (H^o)	3.6 ± 1.4	-40.2 ± 0.5	7.1 ± 1.5
		H168α (HII)	2.7 ± 0.5	-42.9 ± 1.3	26.6 ± 3.8
		C168α	5.3 ± 1.3	-39.7 ± 0.4	5.5 ± 0.9
		S168α	1.9f1.1	-48.3f1.4	8.0 ± 3.4
2	W3B	H168α	0.5 ± 0.1	-40.8 ± 0.6	6.3 ± 1.5
3	W3C+D	H168α	0.6 ± 0.2	-46.6 ± 1.4	22.4 ± 3.8

carbon line emission observed from **W3A** seems to be affected on the negative velocity side by another spectral line. This has been identified as the recombination line of sulphur (Pankonin *et.al.* **1977).** It is interesting to note that in the spectra towards **W3A** obtained by us and in other interferometric observations (*e.g.* Roelfsema 1987), the narrow H168α line is observed to be stronger than the broad H168α, near **20** cm. This is unlike the result from single-dish ,observations of Pankonin *et.al.* **(1977)** in which they observed a stronger broad hydrogen component and a relatively weak narrow component towards **W3.** This is probably because in the large beam ($\sim 9'$) of the single-dish observation, the narrow hydrogen line from **W3A** is beam-diluted whereas the broad line contains contributions from other **W3** components.

Although the primary beam at **20** cm **(30')** was sensitive to radiation from the entire **W3** region, we concentrate on the emission from **W3A** since this is the only HII region from which the carbon line is detected. Fig **6.4** shows the continuum emission across **W3A** after smoothing to a resolution of **10" x 10".** The rest of the discussions, unless specified otherwise, are based on the line and continuum images of **W3A** with a resolution of **10"** x 10".

The line emission displays considerable variation across W3A. Line profiles at a few selected pixels are shown in Fig **6.5.** In Fig **6.5** (a), a typical pixel from the north of **W3A** is shown where an additional spectral feature at a radial velocity of **17** kms^{-1} with respect to the H168α is detected. The width of this feature is $\sim$ **18** kms^{-1}. The gas giving rise,to this line is unlikely to be associated with **W3A** and most probably is a cloud along the line of sight. Roelfsema **(1987)** reported a positive velocity H166α from the southern parts of **W3A** with a width of $\sim$ 22 kms^{-1} centred at about *6* kms^{-1}.

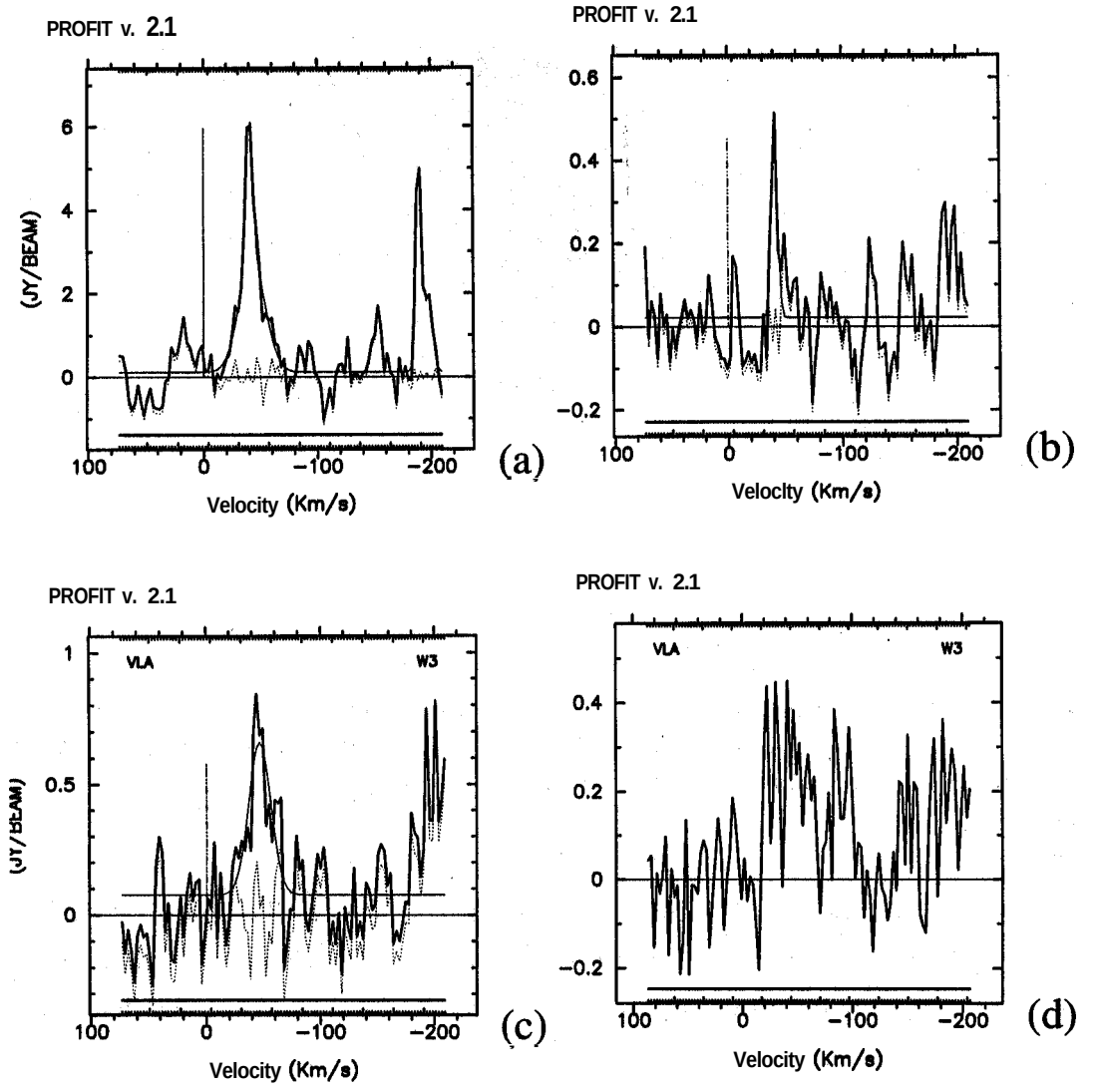

Figure 6.3 The 168α global spectra over W3A (a), W3B (b), W3C+D (c) and W3H (d). The Gaussian fits to the first three are superposed as smooth curves on the observed profiles.

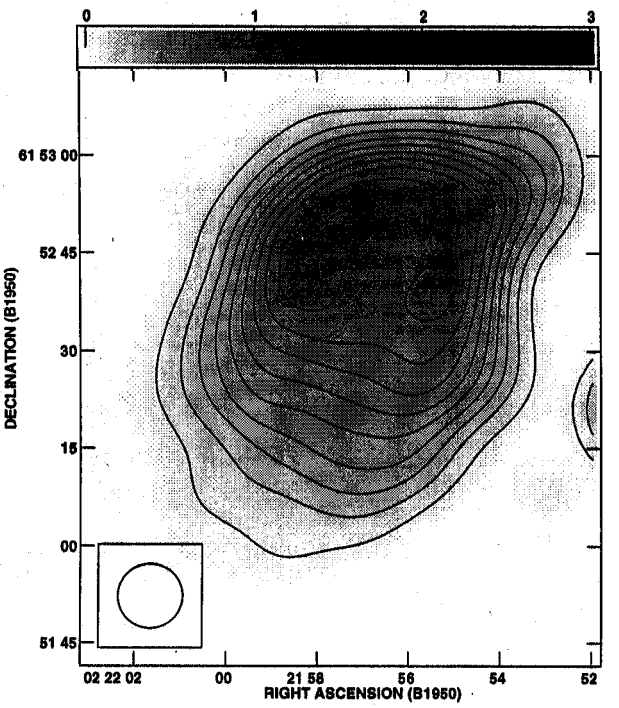

Figure 6.4 **Continuum image of W3A at 1.375 GHz with an angular resolution of 10" x 10" and P.A. = 0°. The grey scale ranges from 0 to 3 Jy/beam. The contours levels are 1,2,3,4,5,6,7,8,9,9.9 in units of 110 mJy/beam.**

We do not observe any such line in the southern parts of W3A. The positive velocity component shown in Fig 6.5(a) is observed only over a small northern region of W3A. Emission at a typical pixel in W3A where the carbon line brightness exceeds that of the hydrogen line brightness is shown in Fig 6.5(b). The sulphur line is also intense in this region. In Fig 6.5(c), the spectrum from the northwest extension in W3A from where some of the broadest hydrogen lines are observed is shown - the broad hydrogen line has a width ~ 70 kms^{-1}. The spectrum shown in (d) is at the peak of the continuum emission. One can see that the broad hydrogen emission is strong here.

In Fig 6.6 (a), the H168α emission across the continuum shell of W3A observed at different radial velocities is shown. These images contain contributions from both the narrow and the broad hydrogen components. The Fig shows that the position of the peak in the H168α emission shifts as the radial velocity is changed.

The channels which show carbon and sulphur line emissions across W3A are shown

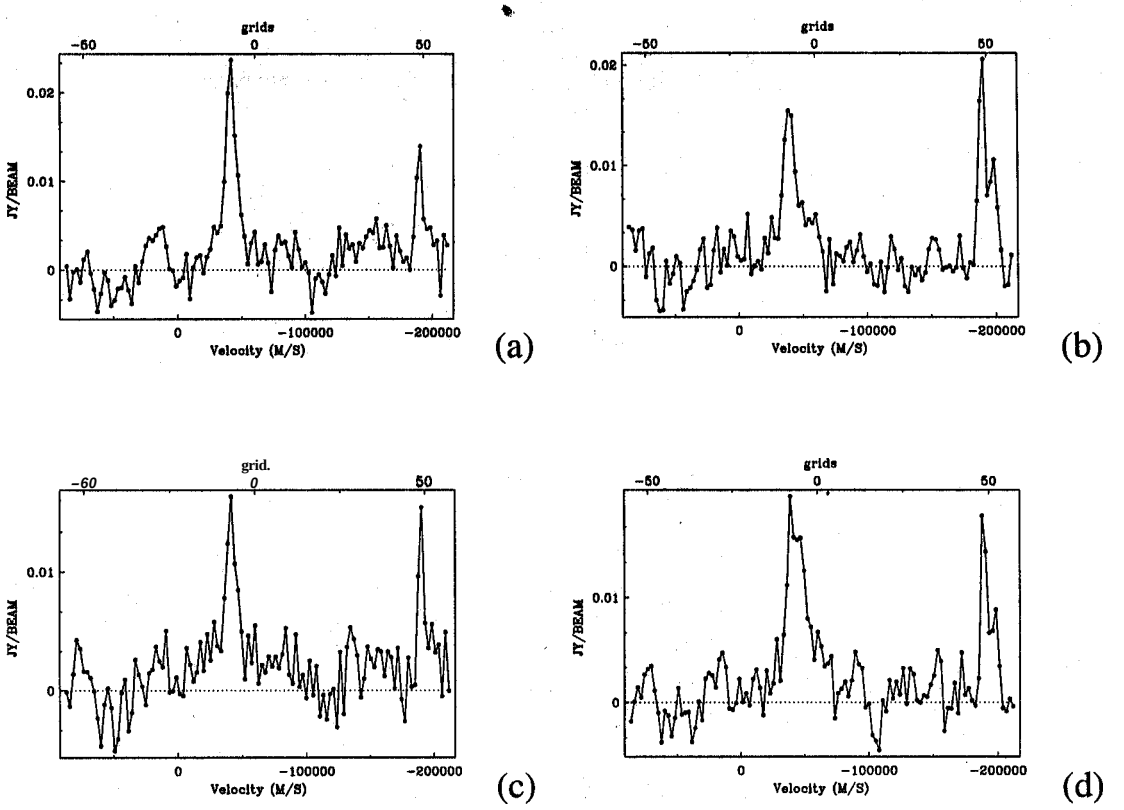

Figure 6.5 Spectra at four typical pixels in **W3A** are shown. (a) **A** pixel in the north of **W3A** is shown where a spectral feature at a positive velocity is detected. (b) **A** pixel in the south of **W3A** is shown where the carbon line is more intense than the hydrogen line. (c) A typical pixel from the north-west extension of the continuum source is shown where the broadest ($\sim$ 70 $\mathbf{kms^{-1}}$) hydrogen lines are observed. (d) In this spectrum on a pixel with the peak continuum emission, the broad ($\sim$ 25 $\mathbf{kms^{-1}}$) hydrogen line is relatively stronger.

in Fig *6.6* (b). The emission observed at radial velocities of -38.3 and -41 $\mathbf{kms^{-1}}$is due to transitions in carbon whereas the emission at velocities near -48.9 $\mathbf{kms^{-1}}$is due to sulphur. The emission due to sulphur is weak compared to the carbon line emission.

In order to compare the spatial distribution of H^{o} and CII regions, it is necessary to separate the narrow hydrogen line from the broad hydrogen line in the images shown in Fig 6.6 (a) and carbon line from the sulphur line in Fig 6.6 (b). This separation was achieved by fitting four Gaussian components to the line profiles at each pixel in the W3A line cube. The Gaussian fits were made using the procedure PROFIT in the Groningen Image Processing System (GIPSY) (van der Hulst *et.al.* 1992). The four Gaussian components corresponded to the broad hydrogen line, the narrow hydrogen

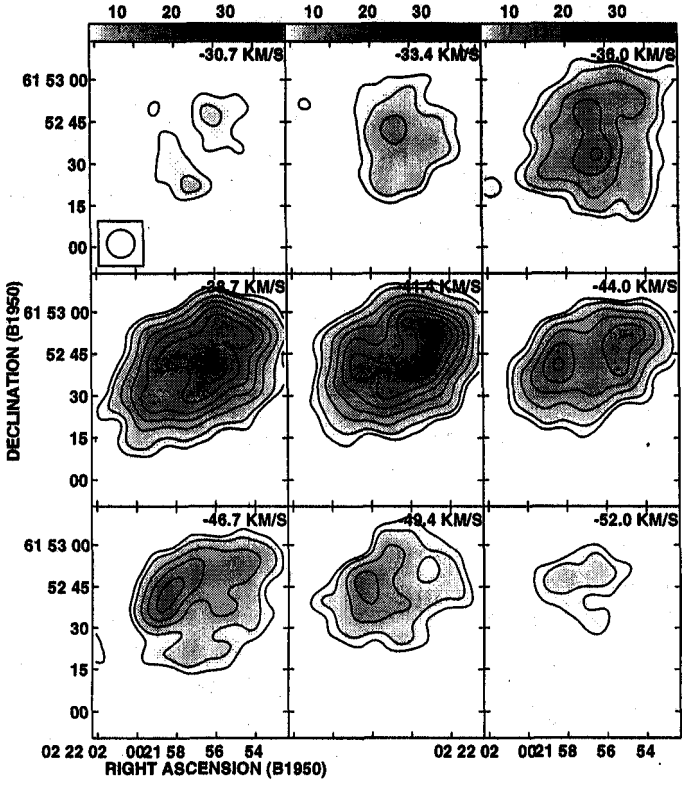

Figure 6.6 (a) The distribution of H168α across the continuum source W3A at radial velocities ranging from -31 to -52 $kms^{-1}$are shown here. Contributions from both the narrow and broad components are included. The grey scale flux range is from 5 to 40 mJy/beam. The contour levels are 1.5,2,3,4,5,6,7,8,9,10 in units of 3 mJy/beam

line, the carbon line and the sulphur line. For the four Gaussian, there are 12 free parameters to be fitted to the spectrum at each pixel. At several pixels where lines were weak, we found that the fitting procedure became unstable if all the parameters were kept free. In order to avoid this and to obtain reasonable fits at all the pixels, we fixed some of the line parameters at values which were obtained from the fit to the global profile (Fig 6.3). The width of the narrow hydrogen line was fixed at 7 $kms^{-1}$and the centroid of the broad line at -43 kms^{-1}. The centroid and the width of the sulphur line were held constant at -197.6 kms^{-1}(w.r.t. hydrogen line) and 6.5 kms^{-1}respectively. Since no line emission was detected outside the continuum source, Gausaians were fitted to the spectra only where the continuum intensity exceeded 400

mJy/beam in the image shown in Fig 6.4. The above procedure generated spatial distributions of the peak intensity, widths and centroids of 168α line emission across W3A. These are shown in Figs 6.7 (a), (b) & (c).

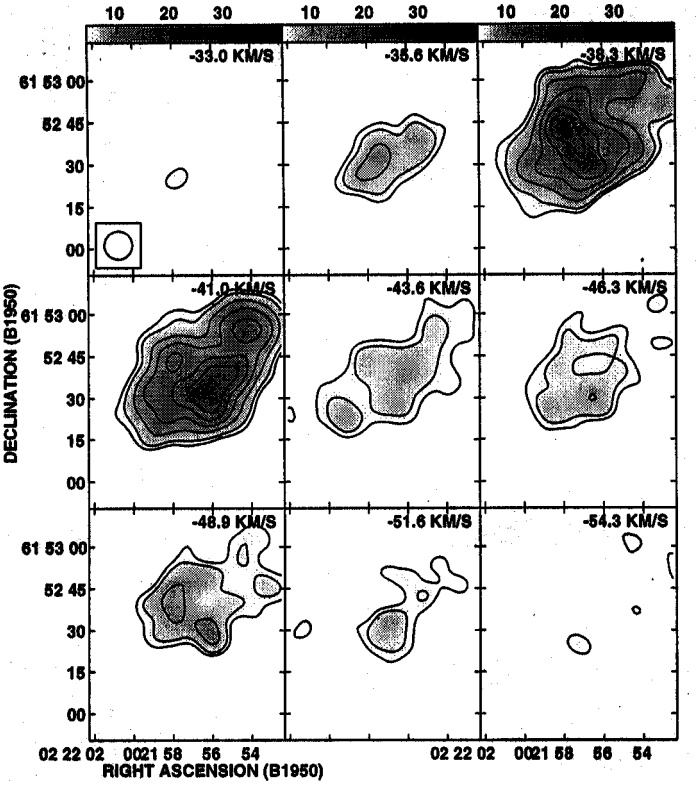

Figure 6.6 (b) The distribution of C168α & S168α across the continuum source in W3A at radial velocities ranging from -33 to -54 kms^{-1} are shown here. To get the radial velocity of S168α, add 8.5 kms^{-1}. Strong carbon line emission is observed at velocities of -38.3 and -41.0 kms^{-1}. The emission at -48.9 kms^{-1} is due to Sulphur. The grey scale coding and contour levels are as in (a).

Fig 6.7 (a) shows that the broad and narrow hydrogen lines trace entirely different distributions over the continuum source. The carbon and the narrow hydrogen line intensities also display different morphologies. However, the carbon and sulphur line intensities seem to show some structural similarities over the continuum source. The intensity distribution of the broad line resembles the morphology of the continuum over W3A. The peak line emission coincides with the peak continuum emission. These

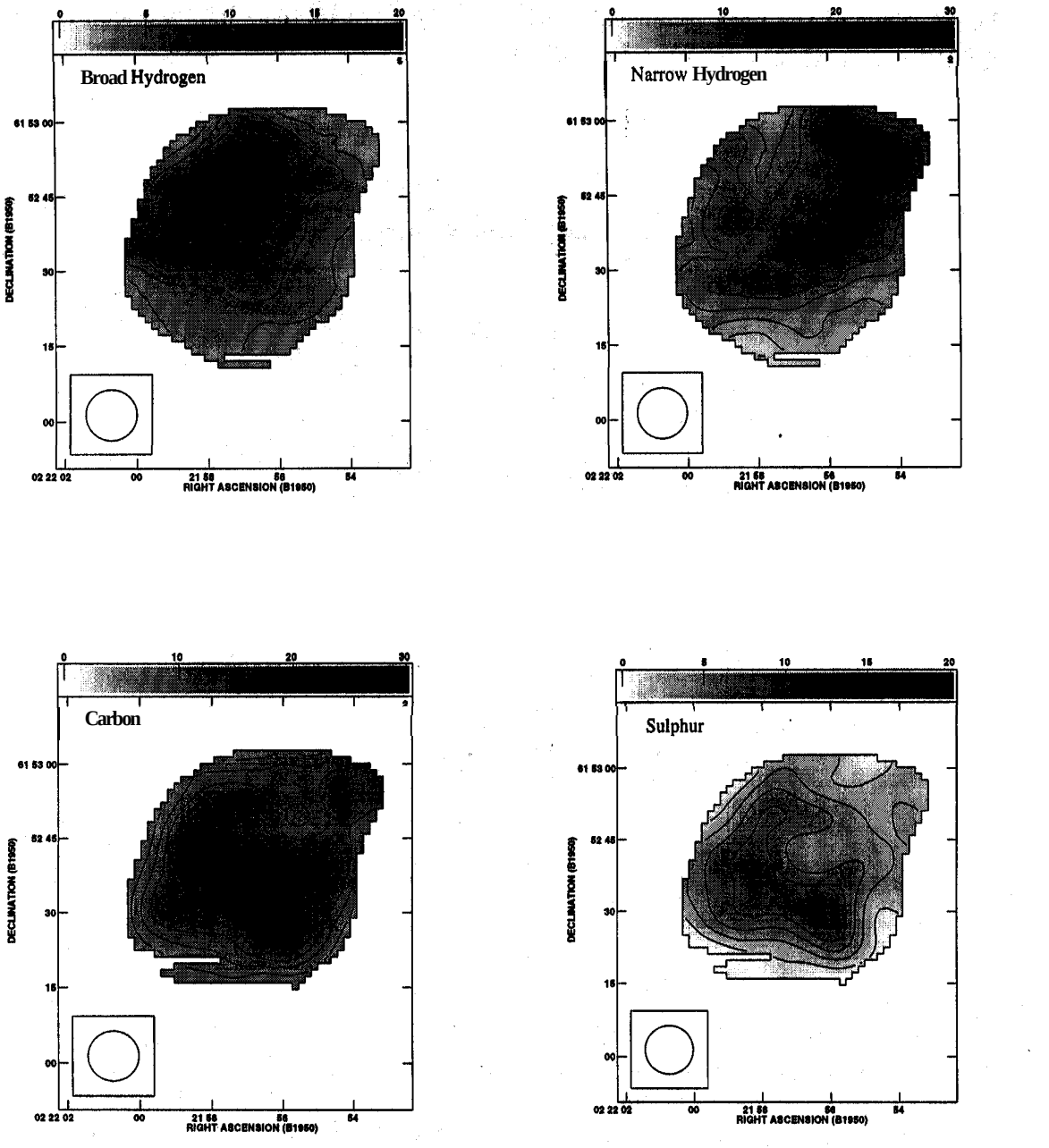

Figure 6.7 (a) Peak line intensity distributions of broad and narrow H168α, C168α, S168α across W3A obtained from Gaussian fits to the emission at each pixel are shown here. The grey scale flux range ranges from 0 to 20 mJy/beam for the broad hydrogen and sulphur distributions and from 0 to 30 mJy/beam for the narrow hydrogen and carbon line distributions. The contour levels for the broad hydrogen distribution are 4,6,8,10 and 12, for the narrow H168α are 2.5, 5,7.5, 10, 12.5, 15, 17.5, 20, for the carbon line are 9,11,13,15,17,19,21,22 and for the sulphur line are 2,4,6,7,10 in units of 1 mJy/beam.

similarities indicate that the gas giving rise to the thermal continuum is the same as the gas giving rise to the broad hydrogen line. The C168α emission peaks in the south-west and north-west regions of W3A. An enhancement in the C168α emission is also observed from the north-west of the source where W3A is probably breaking out of the parent molecular cloud (Roelfsema *et.al.* 1987). Peak emission of narrow H168α is seen in the same region.

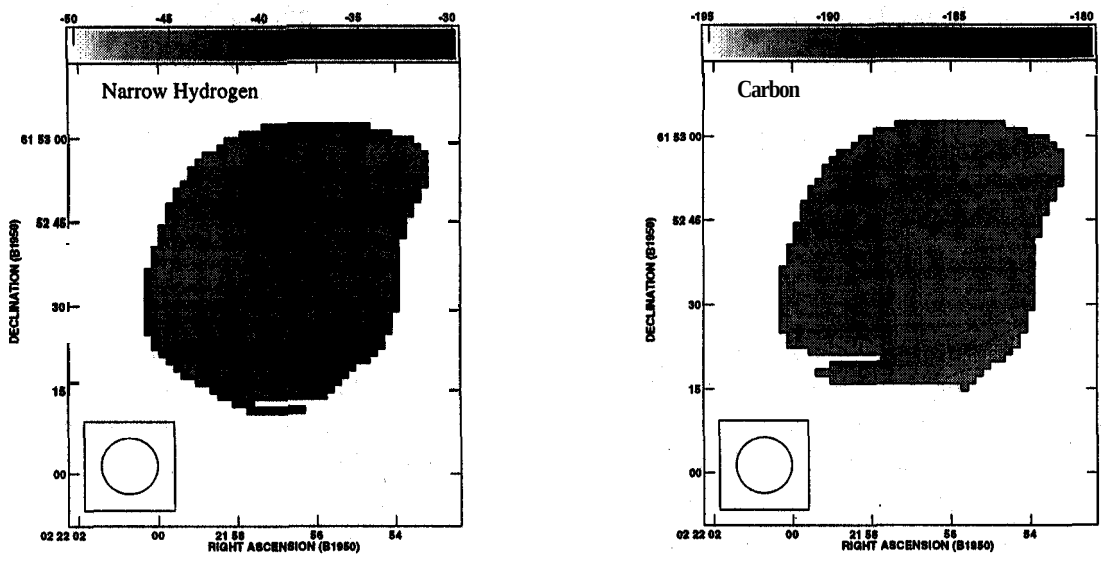

Figure 6.7 (b) The distribution of radial velocities of the narrow H168α and C168α lines. The grey scale flux ranges from –50 to –30 $kms^{-1}$for the H168α and from –45.5 to –30.5 $kms^{-1}$for C168α line distribution. The contours are drawn at –42, –41, –40, –39, –38, –37 $kms^{-1}$for H168α distribution and at –42, –41.5, –41, –40.5, –40, –39.5 kms^{-1}in case of C168α.

Fig 6.7 (b) shows the radial velocity distributions of the narrow H168α and C168α emissions. They do not show any obvious correlation. The narrow hydrogen line velocity shows a gradient across W3A with more positive velocities towards the south. The carbon line velocities, on the other hand, are fairly uniform over the source. The distribution of widths of the observed broad H168α and C168α over W3A are shown in Fig 6.7 (c). The width of the C168α line varies from 4 kms^{-1}in the north to 10 kms^{-1}in the south-east. The width of the broad hydrogen component varies between 15 and 70 kms^{-1}across W3A with the widest ($\sim$ 70 kms^{-1}) lines originating in the northern regions of W3A. The increased widths of the hydrogen line towards the north-west supports the picture of the HII region expanding into a tenuous medium in that region.

Fig 6.8 shows the distribution of the line-to-continuumratio $\frac{S_l}{S_c}$ for the broad H168α,

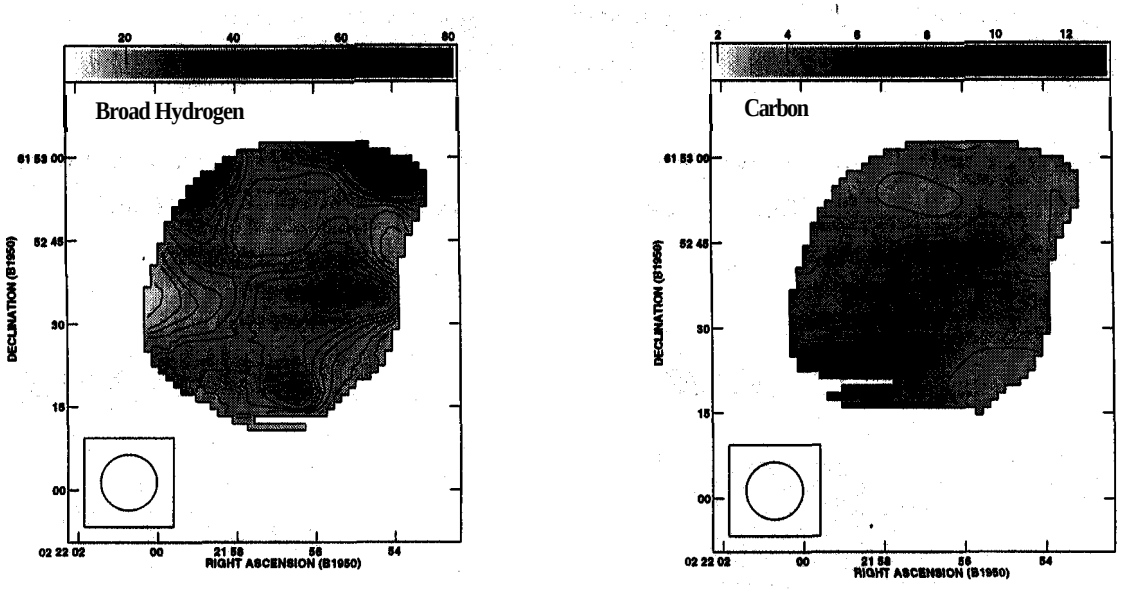

Figure 6.7 (c) The distribution of the widths of the broad H168α and C168α lines across W3A. The grey scale representing widths, ranges from 10 to 80 $kms^{-1}$for the broad hydrogen line and from 2 to 13 kms^{-1}in the carbon line distribution. The contours are drawn for hydrogen line widths of 15,20,22,24,26,28,30,35,40,45,50,60,70 $kms^{-1}$and drawn for carbon line widths of 4,5,6,7,8,9,10 kms^{-1}.

the narrow H168α and the C168α line over the continuum source in W3A. The ratio is expected to be uniform over the continuum source if the same gas was responsible for both the line and continuum emission. Alternatively, the ratio would be uniform if the line-producing gas was homogeneous and stimulated emission of the background radiation was the main emission mechanism. Any structure displayed by the emission in the second case could be due to variation in the physical properties of the foreground gas. The line-to-continuum ratio of the broad H168α line is fairly constant over the source. The widths ($\sim$ 27 kms^{-1}) of these lines and the uniform ratio $\frac{S_l}{S_c}$ seem to indicate that the line and the thermal continuum arise in the same hot gas. However, the distribution of the line-to-continuum ratio of the narrow H168α and C168α lines over the continuum disk exhibit interesting structure (See Fig 6.8 (b) & (c)). The ratio $\frac{S_l}{S_c}$ of the narrow H168α line peaks in the north-west corner of the continuum source and decreases along a ridge which runs towards the south-east. Regions of decreased $\frac{S_l}{S_c}$ are observed in the north-east and south-west parts of the continuum source. On the other hand, enhanced $\frac{S_l}{S_c}$ of the C168α line is seen towards the north-western edge similar to the narrow H168α but in addition, the ratio also peaks in the regions south of the centre of W3A. A depression in $\frac{S_l}{S_c}$ is observed in a region slightly north-west of

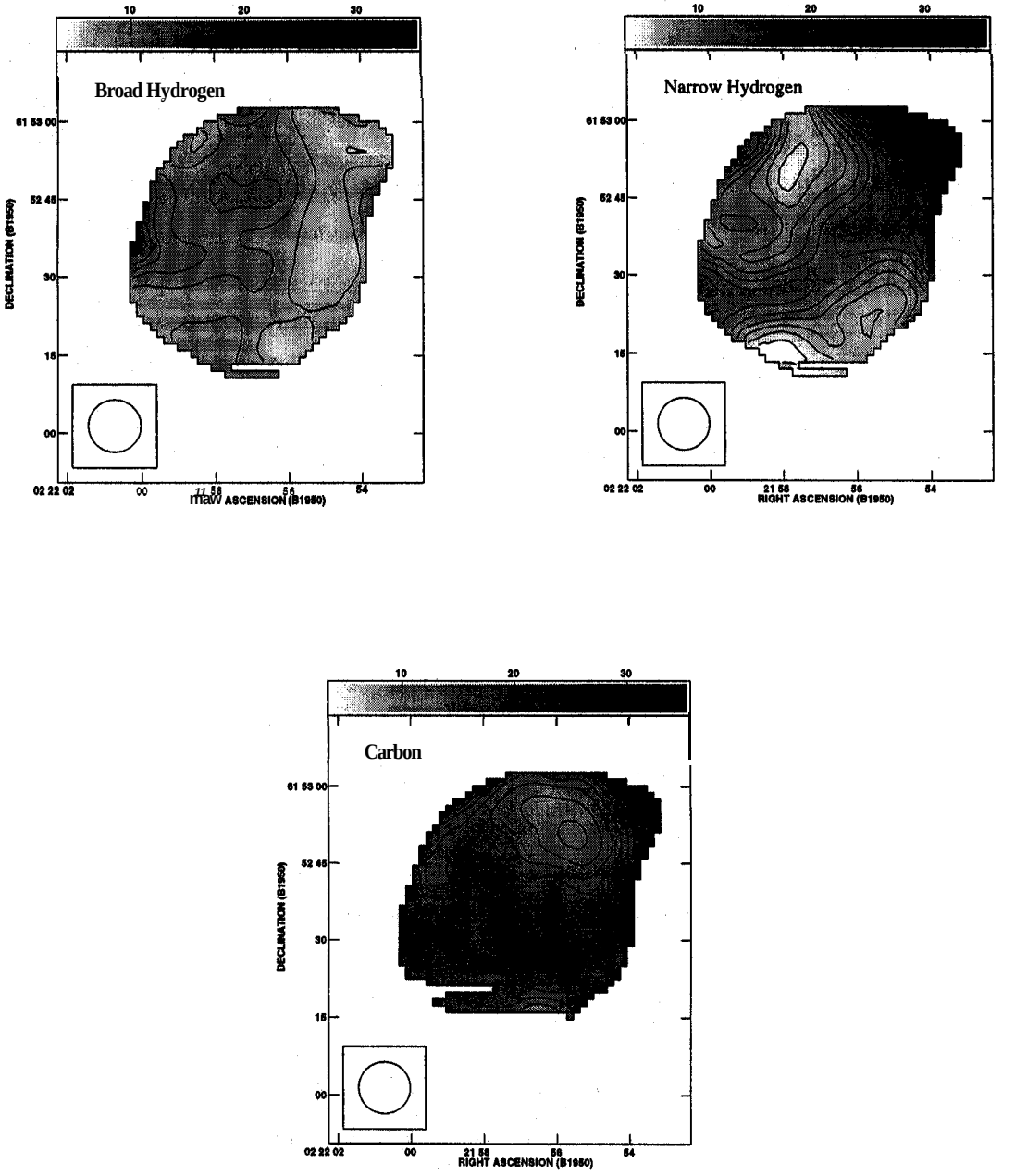

Figure 6.8 The distribution of the line-to-continuum ratios of the broad H168α, narrow H168α and the C168α lines over the continuum source. The grey scale flux ranges from 4 x 10^{-3} to 35 x 10^{-3}. The contour levels are 5,7,9,11,13,15,17,19,21,23,25,27,29,30 in units of 1 x 10^{-3} for all the three distributions.

the centre.

6.3 The Partially Ionized Medium

The broad H168α emission arises in the hot, ionized nebula of W3A. However, the widths of the narrow H168α and C168α lines rule out their origin in the hot HII region and the lines originate in the partially ionized medium associated with the HII region. In this gas, hydrogen is likely to be partially ionized though carbon could be fully ionized. Since the hot HII region is optically thick at 20 cm ($\tau \sim 2.3$ at the peak of continuum emission) over most parts of W3A, the C168α and H168α lines can only arise from the near side of the HII region. In the rest of the discussion, we refer to the narrow hydrogen lines as H° lines. The carbon lines are referred to as CII lines.

6.3.1 Spatial Distribution of Hydrogen & Carbon line regions

If the narrow lines were arising in a homogeneous, isothermal partially ionized layer in front of the HII region, then the distributions traced by the carbon and hydrogen lines should have resembled the continuum distribution since stimulated emission is expected to be the main mechanism (Pankonin *et.al.* 1977). But as the distributions do not trace the continuum (Fig 6.7 a), the structure observed in the CII and H° lines can only be explained by variations in the physical conditions (n_e , T_e or emission measure) of the foreground region over W3A (see also Roelfsema *et.al.* 1987). Furthermore, since the distributions traced by the C168α and the narrow H168α lines over W3A are themselves different, it may indicate different physical properties in the H° and CII regions. However, the correlation observed between the two distributions near the north-west edge and along the ridge extending to the south-west (see Fig 6.8 b) suggests regions of overlap. It thus appears that the narrow H168α & C168α line emissions which originate in a layer lying in front of the HII region, share some overlap but they are not entirely coextensive. The images in Figs 6.8 (b) & (c) which are displayed with the same contour levels and grey scales show that large line-to-continuum ratios ranging from 0.011 to 0.023 are observed in the C168α line over the entire continuum source. Even larger values ($\sim$ 0.029) occur in the north-west region. Compared to these, the ratios observed for the narrow hydrogen line range from 0.005 to 0.015 over most of the source, reaching upto 0.027 in the north-west regions. The carbon line emission is thus more intense than the narrow hydrogen emission. Moreover, strong carbon line emission is observed over the entire continuum source unlike the hydrogen line which is mostly confined to a ridge running across the source. These differences

are suggestive of a structure where the hydrogen line is emitted only from a thin, possibly, patchy layer of partially ionized medium (PIM) just outside the H II region. The carbon line, on the other hand, is emitted both from this region as well as from the photodissociation region (PDR.) (Tielens & Hollenbach 1985) which extends to larger depths in the parent molecular cloud. In the PDR, the stellar ultraviolet radiation field (6 − 13.6 eV) is sufficient to keep carbon (ionization potential = 11.4 eV) ionized but is not strong enough to ionize hydrogen (ionization potential = 13.6 eV). Thus, since carbon is likely to be fully ionized to larger depths in the neutral gas compared to the partially ionized hydrogen region, the narrow H168α line would be weaker and is expected to have a different spatial distribution compared to the C168α line.

Anantharamaiah *et.al.* (1990) have imaged the H II region Orion B in the narrow hydrogen and carbon line emission and inferred that the C II and H° regions are spatially coincident, confined to a small area of the continuum source. This result is somewhat different from what we obtain for W3A where C II and H° share some overlap and are seen over almost the entire continuum source. However, Anantharamaiah *et.al.* (1990) find the C II emission to be more widely-distributed over Orion B than the H° emission which is not unlike the result we obtain for W3A. Furthermore, they find that the emission due to an element heavier than carbon, possibly sulphur over Orion B has a distinct distribution. In the case of W3A, the C168α and S168α emission show good correspondence.

6.3.2 Expansion in the North-west region

As mentioned above, an enhancement in the line-to-continuum strength is observed in the H° and C II lines towards the north-west extension of W3A. Roelfsema *et.al.* (1987) had noted the excess emission in C168α from this region and attributed the enhanced emission to ultraviolet photon leakage from the H II region. Dickel *et.al.* (1983) also noted strong [0111] emission from this region, which requires large intensity of ultraviolet photons. Roelfsema *et.al.* (1987) suggest that at this position, the H II region is breaking out from its parent molecular cloud and has become density bound leading to increased ionization and hence stronger spontaneous C168α emission. The increased fractional ionization of hydrogen in the PIM seems to be producing the same effect in the narrow H168α emission which peaks in this region. Furthermore, the broad H168α lines observed from this region are the widest as seen in Fig 6.7 (a), again providing evidence for expansion. The central velocities of the H° (−41 kms^{-1}) and C II (−40.5 kms^{-1}) lines are slightly more negative in this region as compared to most of the source, supporting the theory that the matter in this region is moving towards us (Roelfsema

et.al. 1987).

6.3.3 Comparison with other tracers

We compared the recombination line distribution with the optical depth maps of H_2CO which sample the molecular gas between us and the HII region. A slight increase in the optical depth of H_2CO (Arnal *et.al.* 1982) at -40.5 kms^{-1} is observed near the north-west extension. Enhancement in the H_2CO optical depth is also observed in the area located south-west of the centre of W3A at a velocity of -40 kms^{-1}. This partially overlaps with the region where a peak in the optical depth of C168α is observed at the same velocity. Absence of a similar increase in the H° line emission in this region suggests that the enhanced carbon recombination line emission from the southern regions is not associated with the PIM but with the molecular clumps seen in H_2CO in the PDR. Furthermore, H_2CO displays low optical depth in the northern region at -40.5 kms^{-1} which coincides with the dip seen in the C168α emission in the line-to-continuum image in Fig 6.8 (c). In the previous section, it was shown that a fraction of CII emission certainly originates in the PIM. The similarity shown by CII with the molecular gas structure indicates that part of this emission also arises in the PDR. It is therefore clear that the H^{o} line emission is confined to the PIM whereas the CII line emission arises both in the PIM and the PDR associated with the HII region in W3A.

We also searched for correlation between the C168α recombination line and the [CII]158μm fine-structure emission line across W3A since both involve ionized carbon and also because the process of dielectronic-like recombination which influences the electronic level populations in carbon is an exciting mechanism for the fine-structure transition (Watson, Western & Christensen 1980, hereafter WWC80). The W3 region has been imaged in [CII] line by Howe *et.al.* (1991) with a resolution of 55″. Unlike the C168α line emission, the [CII] emission is detected from the entire W3 complex with enhanced emission near W3B. No increase in [CII] emission is seen near W3A. However, strong C168α line is observed from W3A. This difference indicates that the predominant contribution to the two lines may be from different phases of the ISM. Howe *et.al.* (1995) have concluded that the 158 μm fine-structure line observed from star-forming regions arise on the surface of molecular clumps. However in recent separate studies, Petuchowski & Bennett (1993) and Heiles (1994) have suggested that most of the observed [CII] lines in the galaxy arise in an extended low-density warm ionized medium (ELDWIM). On the other hand, Bennett & Hinshaw (1993) have attributed the [CII] line to PDRs surrounding HII regions and Shibai *et.al.* (1996) argue that the lines arise in the cold neutral atomic gas (CNM). Since no correlation is observed

between the recombination line and the fine-structure line from W3A with the existing resolution, it appears that the [CII] line observed by Howe *et.al.* (1991) may not be associated with the PDR in W3A. However, high angular resolution [CII] data is required to support this preliminary result.

No meaningful comparison between the C II & H^{o} lines and the 21 cm H I absorption (van der Werf & Goss 1990) could be made since the 21 cm line towards W3A at a radial velocity ~ -40 kms^{-1} is saturated.

6.3.4 Modeling H^{o} & C II regions

The observed line intensity, line width and radial velocity of a recombination line carry information about the physical properties and kinematics of the parent cloud. If expected intensities for a given set of physical conditions can be calculated with the aid of the radiative transfer equation, then comparison with the observed values provide constraints on the properties of the emitting regions. Doppler-broadening of the line gives a measure of the thermal and turbulent motions in the cloud, whereas pressure-broadening of the line gives estimates of the true electron density in the line-emitting gas. The radial velocity of the spectral line is a measure of the kinematic distance to the emitting cloud. By putting together all this, a model of the emitting region can be constructed.

Since the range of physical conditions which can be explored to explain the observed line emission is vast, it is useful to make some simplifying assumptions and constrain the parameter space.

- **Electron temperature from the line widths:** As mentioned before, although the H^{o} and C II regions are not perfectly correlated, there are some regions of overlap like the north-west extension and tie ridge-like region across W3A. Moreover, Onello *et.al.* (1995) have reported a high correlation coefficient between the normalized H^{o} and C II line intensities from their single-dish study of several such regions and interpreted it as due to a common origin with the same excitation mechanism. Thus, for the purpose of estimating an electron temperature of the emitting medium, we assume that both the narrow H168α and the C168α lines arise in the same gas. On this assumption, the contribution of turbulent velocities to the line widths of the two species is the same and the difference in the widths is only due to their different atomic masses. From the measured line width of 7 kms^{-1} for the H^{o} line and 5.5 kms^{-1} for the C II line, we calculated the electron temperature of the gas to be 420 K. The root mean square

turbulent velocity is 4 kms^{-1}. The value we obtain for T_e is somewhat higher than the earlier estimate of 150 K by Pankonin *et.al.* (1977). If we consider the extreme case where the gas is devoid of turbulence, we get upper limits on the electron temperature of 1100 K for the H^o and 8000 K for the CII region.

- Limits on the electron densities from molecular densities and pressure broadening: Typical densities of a few times 10^4 cm^{-3} have been derived for the foreground molecular material in W3A from H_2CO observations (Arnal *et.al.* 1982). However, Henkel *et.al.* (1980) have determined the molecular density in H_2CO clumps to be $\sim 1 \times 10^5$ cm^{-3}. Hence, if as an upper limit, we assume a typical density of 5×10^4 cm^{-3} in the surrounding molecular material (*i.e.* 10^5 cm^{-3} for HI), the hydrogen densities in the PIM and PDR cannot exceed this number as these regions are formed from the dissociation of H_2 molecules followed by photoionization. Hence for the CII region, if the number abundance of carbon is assumed to be 3×10^{-4} with respect to hydrogen and if all the electrons are believed to come from undepleted carbon, then the electron density cannot be in excess of 30 cm^{-3}. If carbon is depleted onto dust grains then this limit will be lower. In the H° region, the electrons may be contributed by both carbon and hydrogen and so the electron densities may exceed this number. If electron densities of a few tens cm^{-3} is contributed by hydrogen, implying a fractional ionization for hydrogen of $\sim 10^{-4}$ then the density would be ~ 50 cm^{-3}. We proceed with the analysis assuming the electron densities to be in the range of $1 - 30$ cm^{-3} for the CII region and in the range $1 - 50$ cm^{-3} for the H° region. An upper limit on the electron density of ~ 150 cm^{-3} in the CII region can be derived if the carbon line width of 5.5 kms^{-1} is assumed to be entirely due to pressure broadening. The molecular densities place a more stringent constraint on the largest possible electron density.

- Limits on the thickness of the foreground PIM region: Roger and Dewdney (1992) have shown that for a uniform density, spherically symmetric HII region excited by a 0 4 star, the surrounding dissociation region will be about 1.5 times the size of the HII region and the size increases as the spectral type becomes cooler. The central star in W3A is believed to be a O6 type (Adler *et.al.* 1996). Assuming that W3A is spherically symmetric and of uniform density and since its linear size is ~ 0.4 pc, we get a size for the dissociation zone of ~ 0.6 pc. Hydrogen is likely to get partially ionized in a part of this photodissociation zone and hence the H° region is expected to be smaller than 0.6 pc. These are useful

limits on the size of the PIM around W3A.

Within the above constraints on the temperature, density and size of the emitting region, we consider two types of models for the C II and H° regions. In the first model only spontaneous emission of the recombination lines is assumed and in the second model, stimulated emission due to the the strong thermal background radiation field from the H II region is also considered. The emission measure and temperature of the H II region are taken to be 1.3×10^7 pc cm^{-6} (Adler *et. al.* 1996) and 9000 K respectively. Since the line-emitting region we are studying is right in front of the H II region, the dilution for the background radiation is 0.5.

We assumed an isothermal, homogeneous line-producing cloud to simplify the modelling although there are obvious inhomogeneities in the line distribution. The line emission at the continuum maximum (0.0058 Jy/beam for H° line and 0.021 Jy/beam for the C II line) was used to constrain the emission measure for various assumed values of density. We regard the variation in line emission across the source to be due either to variation in pathlengths through the gas or to varying electron densities. The departure coefficients b_n and β_n which are a measure of the deviations of the level populations from LTE were calculated from the computer code of Salem & Brocklehurst (1979) which has been modified by Walmsley & Watson (1982) to include the effects of dielectronic-like process (WWC80) and further modified by Payne, Anantharamaiah & Erickson (1994) to extend the calculation to large quantum numbers ($n > 1000$). Considerable influence is exerted by the dielectronic-like recombination process on the level populations in carbon in regions where the free electron energies exceed 92 K (WWC80). This process involves the excitation of the fine-structure states ($^2P_{3/2}, ^2P_{1/2}$) in the ground state of carbon by the recombining energetic electron. To calculate the abundance of gaseous carbon, we used a depletion factor of 0.5. The radiative transfer equation was solved for $T_e = 420$ K and n_e ranging from $1 - 30$ cm^{-3} for C II region and n_e varying from $1 - 50$ cm^{-3} for the H° region. The resulting emission measure and pathlength through the gas required to explain the observed line emission at the continuum maxima are listed in Table 6.3.

All the spontaneous emission models which are listed in columns 4 & 5 of Table 6.3 require pathlengths which are more than an order of magnitude larger than the size of the H II region. This is inconsistent with the photo-dissociation model of Roger & Dewdney (1992). We, therefore rule out models in which the line emission near 20 cm is due to spontaneous emission. In the stimulated emission models, the pathlengths required to explain the narrow hydrogen line is in the range $0.5 - 0.02$ pc for electron

Table 6.3 **Probable physical parameters of the H° and CII regions in W3A**

$T_e = 420K$						
			Only Spontaneous Emission		Spontanous + Stimulated Emission	
No	Line	N_e cm^{-3}	EM pc cm^{-6}	L pc	EM pc cm^{-6}	L pc
1	H168α	1	2943	2943	11.7	11.7
		5	2697	10.8	11.5	0.5
		10	2935	29	14.4	0.14
		20	3420	8.5	20.8	0.05
		25	3630	5.8	24	0.04
		30	3827	4.3	27	0.03
		50	4486	1.8	40	0.02
2	C168α	1	5315	5315	65.7	65.7
		5	6112	245	77.4	3.1
		10	7010	70.1	99	0.99
		20	8508	21.3	144	0.36
		25	9132	14.6	165	0.26
		30	9725	10.8	186	0.21

densities in the range of 5–50 cm^{-3}. Electron densities < 5 cm^{-3} can be ruled out since pathlengths much longer than the Roger-Dewdney limit are required. Using similar arguments, the observed carbon line strengths are explained by stimulated emission models with n_e in the range $20 - 30$ cm^{-3}. The corresponding path lengths are $0.36 - 0.21$ pc. However, since the C168α emission arises both in the PIM and the PDR, the Roger-Dewdney limit is not strictly applicable to the CII regions and the electron density can range from 1 to 30 cm^{-3}. The temperature in the CII region associated with the PDR is likely to be lower than 420 K but since we have no other constraint on the temperature, we assume a temperature of 420 K obtained from the ratio of line widths.

From the above analysis and from the distribution of the line emission across W3A discussed in the previous section, it is clear that the H° and CII regions are not entirely coextensive and that stimulated emission is the main mechanism for line emission at 20 cm. If both the clouds are at a temperature of 420 K and have electron density in the range of $5 - 30$ cm^{-3}, then the H° cbud is likely to be in the range $0.5 - 0.02$ pc

large whereas the corresponding pathlength through the CII cloud is expected to be $3 - 0.2$ pc. The variation in the line emission observed over the continuum shell can be explained by variations in the electron density in the line-forming region or due to different linear sizes of the clouds. For a temperature of 420 K and electron density of 25 cm^{-3}, we found that the pathlength variations required to explain the narrow H168α line emission ranged from 0.04 to 0.22 pc. On the other hand, the pathlengths through the CII region need to vary from 0.14 to 0.43 pc to explain the observed structure in the emission. We did not attempt to obtain the range of electron densities which would explain the line emission if the path length was held constant since it involved fairly lengthy iterative computation for each pixel in the image.

6.4 The Fully-Ionized HII region

6.4.1 Electron Temperature

At frequencies where a fully ionized HII region become optically thick ($\tau > 1$), the measured continuum brightness temperature approaches the electron temperature of the gas. Therefore, in the case of W3A, which appears to be optically thick at 20 cm, the measured brightness temperature differs from the physical temperature of the cloud by a small correction factor introduced by the finite optical depth *i.e.* $T_b = T_e(1-e^{-\tau_c})$. This correction factor can be derived if a continuum image at a higher frequency where the HII region is optically thin is available. We have obtained such an image at 8.3 GHz from Adler *et.al.* (1996). In Fig 6.9, we show this image alongwith our 1.4 GHz image at the same resolution. The angular resolution in both the images is 5.3'' x 5.2'' and P.A. $= -41°$. In Fig 6.10, we show one-dimensiopal crosscuts across these images passing through the continuum peak. It is clear from the nature of the two crosscuts that the HII region is becoming optically thick near 20 cm.

From the peak brightness determined at 1.4 GHz and 8.3 GHz from Fig 6.10, we calculated an electron temperature of 8758 $\pm$ 216 K using the method given in (Subrahmanyan and Goss, 1996). Using the line-to-continuum ratio of the H92α (8.3 GHz), Adler et.al. (1996) have obtained a temperature close to 8000 K. Since W3A is optically thin at 8.3 GHz, the H92α line samples the entire line of sight, all the way to the interior of the HII region and the emission is expected to be dominated by the high emission measure central regions. On the other hand, the temperature from the optically thick brightness at 20 cm is likely to be characteristic of the outer regions of the HII regions. From the two similar values of the temperatures obtained at these two frequencies, it appears that W3A is isothermal.

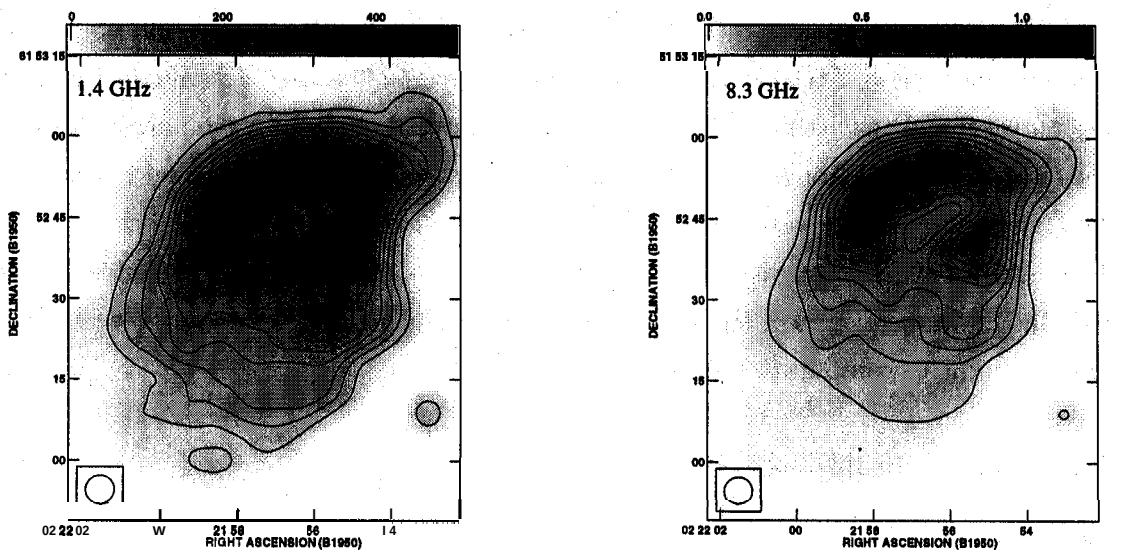

Figure 6.9 The continuum brightness distribution across W3A at 1.4 GHz and 8.3 GHz at angular resolution of 5.3" x 5.2" and P.A. = −41°. The beam is shown in the bottom left hand side corner. The grey scale in the 1.4 GHz map ranges from 0 to 0.5 Jy/beam whereas in the 8.3 GHz map, it ranges from 0 to 1.2 Jy/beam. The contour levels are 1,2,3,4,5,6,7,8,9,10 in units of 37 mJy/beam in the 1.4 GHz map and in units of 79 mJy/beam in the 8.3 GHz map.

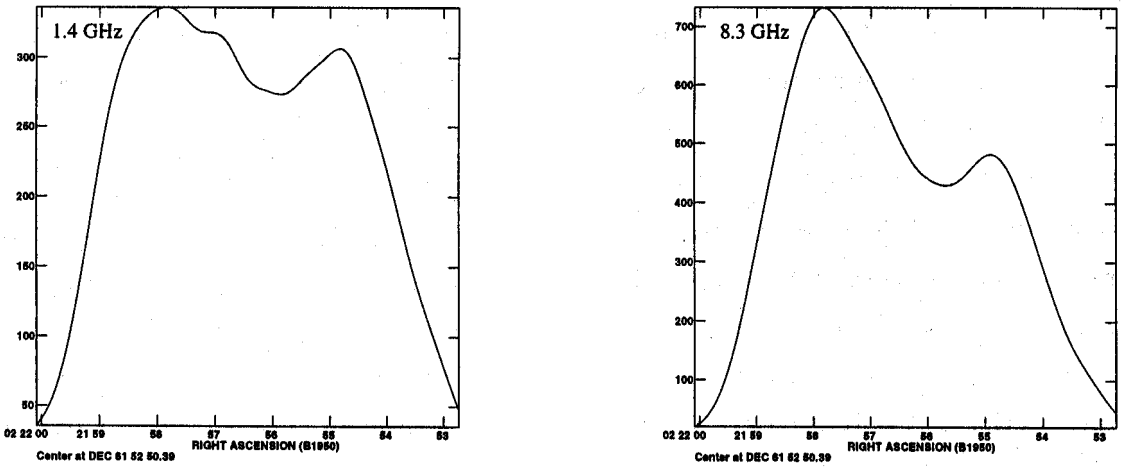

Figure 6.10 Crosscuts across the continuum maps of W3A at 1.4 & 8.3 GHz passing through the peak brightness point.

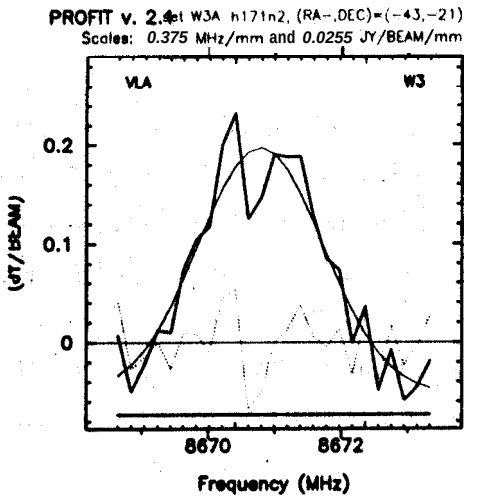

Figure **6.11 The integrated H171η spectrum observed towards W3A is shown here (unpublished data from Juan Uson & W.M.Goss).**

6.4.2 Electron density and Filling Factor

If the HII region W3A is assumed to be a homogeneous spherical cloud, than the observed continuum flux density at a frequency at which the region is optically thin can be related to the average electron density in the region by the following formula given by **Mezger & Henderson (1967):**

$$\left(\frac{n_{e,rms}}{cm^{-3}}\right) = u_1 \; a^{1/2} \; 6.351 \times 10^2 \left(\frac{T_e}{10^4 K}\right)^{0.175} \left(\frac{\nu}{GHz}\right)^{0.05} \left(\frac{S_\nu}{Jy}\right)^{0.5} \left(\frac{D}{kpc}\right)^{-0.5} \left(\frac{\theta_G}{arcmin}\right)^{-1.5} \qquad (6.1)$$

where

a = ratio of the exact formula (Oster **1961)** to the approximate formula (Altenhoff *et.al.* **1960)** of the continuum optical depth

u_1 = density distribution model (*e.g.* spherical, cylindrical or Gaussian)

S_ν = continuum **flux** density of the source at the frequency ν, Jy

D = distance to the source, kpc

$\theta_G = \sqrt{\theta_\alpha \theta_\delta}$, arcmin

The continuum **flux** density of W3A at 8.3 GHz obtained from the image in Fig **6.9** is **23 Jy** and the angular size is $\sim 50''$. Taking d = **2.4** kpc & T_e = **9000 K,** we get $n_{e,rms}$ = **2200 cm^{-3} .** This is clearly a lower limit to the true electron density in W3A since the intensity distributions in Fig **6.9** indicates density inhomogeneities.

Pressure-broadening is a sensitive function of the principal quantum number n and the true electron density $n_{e,true}$ as discussed in Chapter 2. Hence, if a pressure-broadened recombination line can be observed from the HII region W3A, then the true electron density in that region can be estimated. Using this true electron density and the root mean square electron density, the filling factor of the HII region can also be determined. Such a spectrum was obtained by Uson & Goss (private communication) as a byproduct of their observation of ^{3}He towards W3A. The spectrum is shown in Fig 6.11. This spectrum corresponds to the H171η line produced by a transition between n = 178 to n = 171 near 8.76 GHz in W3A. The line is centred near -27 kms^{-1} and has a width of $\sim$ 77 kms^{-1}. If we assume that this line arises in the HII region W3A and that it is pressure broadened, then the line width translates to a true electron density of 2×10^4 cm^{-3}.

The clumpiness in a medium is characterized by the filling factor which is defined as $\epsilon = (n_{e,rms}/n_{e,true})^2$. From $n_{e,rms} = 2200$ cm^{-3} and $n_{e,true} = 2 \times 10^4$ cm^{-3}, $\epsilon \sim 0.01$ for W3A. However, since $n_{e,rms}$ is a lower limit to the average electron density, this value is a lower limit on the filling factor. For most HII regions, this factor is found to be in the range of 0.01 to 0.5 (Osterbrock 1989). The low filling factor of W3A can be interpreted in terms of extensive clumping in the gas with most of the ionized matter being concentrated in high-density condensations. This result seems to be appropriate since the low-density cavity blown by the central exciting star IRS 2a and the high emission measure ionization front observed in radio continuum observations of W3A are obvious signatures of density inhomogeneities.

It is interesting to note that if the H171η (8.7 GHz) line discussed above and the broad H168α(1.4 GHz) line observed by us were arising in the same gas then the latter line should have been pressure-broadened by more than seven times the width of H171η line *i.e.* the H168α line near 1.4 GHz should have been $\sim$ 400 kms^{-1} wide! This is because pressure broadening is a $1/\Delta n$. However, since the HII region is optically thick at this frequency, this component from the central hot ionized regions would be unable to escape from the HII region. The broad ($\sim$ 27 kms^{-1}) component observed in the integrated spectrum of H168α from W3A at 20 cm is characteristic of the hot, low-density outer regions of the HII region. The outer regions at 9000 K can at the most have an electron density of 1200 cm^{-3} if the entire line width was assumed to be due to pressure broadening. Alternatively, the widths in these outer regions could be due only to Doppler broadening. In this case, the electron density in these outer regions is $<<$ 1200 cm^{-3}.

6.5 Summary

We used the VLA at 20 cm to observed the HII region W3A in hydrogen and carbon recombination lines. In addition to the usual relatively broad ($\Delta V \sim 30$ kms^{-1}) H168α line from the HII region, a narrow H168α line and a narrow C168α line was observed from W3A. The spatial distribution of the three lines were separated using multi-component Gaussian fits to individual pixels in the image. Analysis of the resulting images has yielded the following results:

- The distribution of C168α and narrow H1689α lines over W3A bear some resemblance indicating partial overlap; the differences in the structure show that they are not entirely coextensive. The narrow hydrogen lines arise only in the partially ionized medium (PIM) whereas the carbon lines arise both in the PIM and in the photodissociation regions (PDR). The distribution of carbon lines also bears resemblance to molecular gas seen in H_2CO.

- An enhancement in the intensities of the narrow H168α and C168α lines is observed from the north-west regions of W3A. The broadest hydrogen lines also arise in this region. Strong [0111] emission which requires intense ultraviolet field has also been observed from this region (Dickel 1983). These data supports the theory (Roelfsema et.al. 1987) that the HII region is breaking out from the molecular cloud into tenuous regions.

- The enhanced C168α emission near W3A has no counterpart in the [CII]158μm fine-structure line. The dominant contribution to the recombination line and the [CII] 158μm fine-structure line appears to be from different phases of the ISM.

- Assuming that the narrow hydrogen and carbon lines arise in the same gas, the temperature is calculated to be 420 K. The observed molecular densities ($\sim 10^5$ cm^{-3}) impose an upper limit on the electron density in the PDR of $1 - 30$ cm^{-3} & in the PIM of $1 - 50$ cm^{-3}. Spontaneous emission models are ruled out by the Roger-Dewdney limit on the size of an atomic region around a 0 6 star. The observed narrow line emission is due to stimulated emission by a background thermal radiation field. Modelling the observed line intensity as being due to stimulated emission, we find that the observed H168α arises in a cloud at $T_e = 420$ K and $n_e = 5 - 50$ cm^{-3}. The pathlengths required range from 0.5 to 0.02 pc which are allowed by the Roger-Dewdney limit. Stimulated emission in a cloud at $T_e = 420$ K and $n_e = 5 - 30$ cm^{-3} can explain the observed carbon line

emission. The pathlengths through the PIM and PDR required for this emission are 3 pc to **0.2** pc; longer than those required to explain the H° lines.

- The broad hydrogen line and the thermal continuum observed near **20** cm arise in the same gas. The temperature of this region is $\sim$ **8700 K.** The true electron density derived from a pressure-broadened H171η line is $\sim 2 \times 10^4$ cm^{-3} and the root mean square electron density derived from the measured continuum flux is $\sim$ **2200** cm^{-3} **.** These values of $n_{e,rms}$ & $n_{e,true}$ imply a filling factor of $\geq$ **0.01** in W3A.

Chapter 7

Summary & Conclusions

In this thesis we have described the results of an observational study of ionized carbon in the Galaxy using low-frequency recombination lines which arise due to electronic transitions at high quantum numbers ($150 < n < 600$). The major part of the thesis is devoted to the study of very low frequency recombination lines which arise in partially ionized gas associated with a widespread cold, neutral component of the interstellar medium. In addition, results of the investigation of a CII region associated with a classical Galactic HII region are also presented.

The beginnings of the main subject of this thesis was the detection of a very low frequency ($\nu \sim 26.13$ MHz) recombination line of carbon, C631α, towards the strong radio source, Cas A by Konovalenko & Sodin in 1980. Since then, many other transitions at higher ($n \sim 800$) and lower ($n \sim 160$) quantum numbers have been observed from this direction. Absence of a HII region in this direction and the deduced physical conditions in the line-forming region suggested that the ionized carbon region in which these lines originated must be cold and tenuous and most likely associated with the neutral gas along the line of sight. Since the first ionization potential of carbon is 11.4 eV (less than that of hydrogen which is 13.6 eV), background ultraviolet photons with $\lambda > 91.2$ nm, which pervade the Galaxy, can keep it singly-ionized even in cold gas which is far from star-forming regions. The low-frequency recombination lines detected from the direction of Cas A exhibited interesting observable properties. The line width increased steeply at higher quantum numbers ($\nu < 115$ MHz) because of radiation and pressure broadening and the lines were in absorption. On the other hand, at higher frequencies ($\nu > 200$ MHz), the lines were fairly narrow and turned over into emission. Study of the behaviour of these lines as a function of frequency yields constraints on the physical parameters of the line-forming region. Such low-frequency lines have also been detected from other directions in the Galaxy. Near 25 MHz, carbon lines have been

detected in absorption from the directions of G75+00, NGC2024, S140, L1407 and DR 21 (Konovalenko 1984, Golynkin & Konovalenko 1990). Lines near 75 & 42 MHz (in absorption) and 328 & 408 MHz (in emission) have been observed from the direction of Galactic centre (Anantharamaiah *et.al.* 1988, Smirnov *et.al.* 1996, Anish Roshi & Anantharamaiah 1997, Pedlar et.*al.* 1978). Towards M16, lines have been observed in absorption near frequencies of 68 & 80 MHz and in emission near 325 MHz (Anantharamaiah *et.al.* 1988). Most recently a search for carbon recombination lines near 76 MHz from the Galactic plane has been rewarding. More than 20 new detections in the inner (galactic longitude $< 20°$) Galaxy have been reported (Erickson, McConnell & Anantharamaiah 1995, hereafter EMA95). This study by EMA95 has shown that the carbon lines are fairly widespread and detectable with the existing low-frequency instruments. The main aim of this thesis was to study such low-frequency recombination lines from the direction of Cas A and from various positions in the Galactic plane at 34.5 MHz (in absorption) using the low-frequency dipole array at Gauribidanur and at 328 MHz (in emission) using the Ooty Radio Telescope and to understand the physical properties of such low-excitation CII regions.

Observation with the low-frequency telescope at Gauribidanur, located $\sim$ 80 km north of Bangalore were central to the work in this thesis. The telescope consists of a 'T'-shaped array of dipoles with a 1.4 km long east-west arm giving an angular resolution of 21' x 25° near 34.5 MHz. The instrument is a transit telescope with minimal tracking facility. Hence, to effectively increase the observing time on a source, an eight-line receiver was used to simultaneously observe eight consecutive transitions (between C571α – C580α) which appeared in the observing band of the telescope. Since, these were the first extensive spectral line observations using this telescope, a new spectrometer with associated hardware and software was developed for this purpose. We were successful in obtaining a high signal-to-noise spectrum towards Cas A with an effective integration time of $\sim$ 400 hours using this telescope. The absorption line displayed distinct Lorentzian wings which is a signature of radiation and/or pressure broadening. Using the measured Lorentzian width, we obtained upper limits on the background radiation field and the electron density of 8000 K and 0.9 cm^{-3} respectively. As mentioned above, this direction, has been extensively studied at various frequencies and the line-forming gas has been modelled. Since Cas A is a very strong background source at all these frequencies, the angular resolution of all the observations is determined by the angular size of Cas A. It is, therefore, possible to compare the different observations directly to constrain the model parameters. We combined our data with other observations to obtain a model which accounts for all the observations. The parameters of the

model are: electron temperature T_e = 75 K, electron density $n_e = 0.03\ \mathrm{cm}^{-3}$, emission measure EM = $0.012\mathrm{cm}^{-6}$ pc, radiation temperature T_{R100} = 3200 K, carbon depletion factor, $\delta_C = 0.9$. The implied thermal pressure in these regions is $n_H T_e \sim 8000\ \mathrm{cm}^{-3}$. Thus the clouds are in rough pressure equilibrium with the interstellar medium. gave a reasonably good. The model parameters suggest that the carbon line region may be associated with the neutral HI gas in this direction. Another check for this hypothesis was conducted by comparing the spatial distributions of C270α (CII), HI 21 cm (atomic hydrogen) and ^{12}CO (molecular hydrogen) lines over the spatial extent of Cas A. For this purpose, we imaged Cas A in C270α ($\nu \sim 332$ MHz) line emission using the Very Large Array (VLA) in its B-configuration with an angular resolution of $\sim 25''$ and the ^{12}CO ($\nu \sim 115$ GHz) line emission using the 10.4 m telescope at Raman Research institute with an angular resolution of $\sim 1'$. The distribution of HI optical depth across Cas A was obtained from published data. The comparison showed that there is good correspondence between C270α & HI distributions and rather poor correlation between ^{12}CO & C270α distributions. This conclusion lends support to the models in which the carbon line-forming regions are associated with the HI gas.

The Gauribidanur radio telescope with the eight-line reliever was used to search for recombination lines of carbon ($n \sim 575$) from about 35 positions in the Galactic plane. We detected carbon lines in absorption near 34.5 MHz from 9 of these directions. The typical line-to-continuum ratios ranged from a few times 10^{-4} to 10^{-3} whereas the typical linewidths varied from 20 to 55 kms^{-1}. On the average, the spectrum towards each position had an effective integration time of ~ 50 hours and a noise level $\Delta T_{rms}/T_{sys}$ of $\sim 2 \times 10^{-4}$. To constrain the physical parameters of the line-forming region, we observed a subset of the 35 positions using the Ooty Radio Telescope (ORT) at 328 MHz ($n \sim 271$) with an angular resolution of $2'' \times 6'$. Emission lines were detected from 9 of the total 14 positions which were observed, including the direction of Cas A. Since the directions observed in the Galactic plane were devoid of strong radio continuum sources like Cas A, the angular resolution of the observation was primarily determined by the telescope beam. At low frequencies, the beams are large and hence the cloud sizes are likely to be smaller than the beam size. The beam-dilution effects which modify the line strengths are thus expected to be important. Moreover different telescopes operating at different frequencies give widely different angular resolutions *e.g.* Gauribidanur telescope has a beam of $21' \times 25^\circ$ and ORT has a beam of $2^\circ \times 6'$. The interpretation of the observed line strength thus depends on the size of the cloud. To obtain some constraint on the size of the line-forming region, the observations with the ORT were made with two different angular resolutions *i.e.* $2^\circ \times 6'$ & $2'' \times 2^\circ$. The

lines that were detected at both angular resolutions had similar line-to-continuum ratios of a few times 10^{-4} and widths ranging from 15 to 55 kms^{-1}. Similar line parameters in the two observations suggest that the line-forming regions are at least 2° x 2° in extent. Furthermore, we attempted to image the fine structure in the cloud towards one of the Galactic plane positions in C270α using the VLA in its D-configuration with a synthesized beam of $\sim 5'$. Although we failed to detect a carbon line from this region, the sensitivity of the observation enabled us to put a lower limit on the structure. The line-forming regions are $> 10'$ in angular extent.

The widths of the lines observed in the Galactic plane at 34.5 MHz and 328 MHz are similar, which is unlike the behaviour exhibited by the lines towards Cas A. This indicates that radiation and pressure broadening, which are both strong functions of n, do not contribute to the line widths at 34.5 MHz for the positions in the Galactic plane. The observed widths are most likely due to differential Galactic rotation. From a model of Galactic rotation, it was deduced that the line-forming gas is distributed between Galactocentric distances of 4 & 7.5 kpc. For obtaining a preliminary idea of the association of ionized carbon in the Galactic plane with other components of the interstellar medium in the inner Galaxy ($l < 17°$), we compared the range of velocities of recombination lines with those at which HI emission & absorption and ^{12}CO emission are seen. HI emission is generally observed at all velocities allowed by Galactic rotation indicating that it is distributed along the entire line-of-sight whereas HI absorption and ^{12}CO are more localized. In most of the cases, we find that the recombination lines appear at radial velocities close to the deepest feature in HI absorption and peak ^{12}CO emission. However we fail to detect carbon lines from other directions which have even higher HI optical depths, which indicates that there are other factors influencing the detectability of the carbon recombination lines. Furthermore, the recombination lines in the inner Galaxy appear over a narrow range of radial velocities as compared to HI emission and in many cases even narrower than HI absorption and ^{12}CO emission indicating that the carbon lines do not arise over the entire line of sight but probably in pockets of gas. From this comparative study it appeared that the recombination lines arise in the partially ionized gas associated with cold neutral gas - either cold HI or H_2. However, it is difficult to distinguish between the atomic and molecular gas in the present study using this test.

The next step in understanding these low-excitation CII regions was to generate physical models for them using the carbon recombination line data. Our carbon recombination line data at frequencies of 34.5 MHz and 328 MHz were combined with the available data at 76 MHz from EMA95. The modelling began by assuming the prob-

able range of temperature, electron density, radiation temperature, fraction of carbon depleted onto grains and the cloud size. The expected variation in integrated optical depth with frequency for various combinations of these parameters were computed and compared with the observed data. To restrict the range of parameters, upper limits on the electron density and radiation temperature were derived from the observed line widths at 34.5 MHz. We considered two types of models. The first one is the cold gas ($T_e \leq 20$ K) model which assume that ionized carbon is caexistent with molecular (H_2) regions and may not be in pressure equilibrium with the interstellar medium. The second type of model is the warm gas ($50 < T_e < 300$ K) model in which the carbon lines are considered to arise in the neutral HI component which is in rough pressure equilibrium with other components of the interstellar medium. The requirement of pressure equilibrium imposes a constraint on the combination of density and temperature used for the models to explain the observed lines. Since non-LTE processes influence the level populations of carbon, it is essential to quantify these effects. The departure coefficients b_n & β_n contain this information. In both types of models, the departure coefficients of various levels in a carbon atom are calculated after including the effect of dielectronic-like recombination process on the populations at high quantum levels in addition to other radiative and collisional processes. The process of dielectronic-like capture, first described by Watson, Western & Christensen (1980), involves the fine-structure levels $^2P_{3/2}$ and $^2P_{1/2}$ of a core electron. An energetic electron (~ 92 K) recombines to a high quantum state of a carbon atom by losing its extra energy to exciting the fine-structure transition. This process has a significant influence on the level populations in carbon, especially in plasma which is close to temperatures ~ 100 K. The computer code of Salem & Brocklehurst (1979) which has been modified by Walmsley & Watson (1982) and also by Payne, Anantharamaiah & Erickson (1994) was used to calculate the level populations in carbon. We tried fitting the observed data assuming three different angular sizes of the line-forming clouds, namely, $> 4°$, $4°$ or $2°$.

The low temperature models could explain the observed variation in optical depth with frequency if the cloud sizes are $> 4°$. The parameters of the fitted models are $T_e = 20$ K, $n_e \sim 0.3\,\mathrm{cm}^{-3}$ and $T_{R100} = 1250$ K and pathlengths of ~ 0.02 pc. Since for most of these positions, the observed data point at 34.5 MHz was not fitted by these models, beam dilution at this frequency translated to a cloud size between $5° - 20°$. However, these models have a shortcoming that the small pathlengths are inconsistent with the observed line widths which are largely due to Galactic rotation. Moreover the models predict large angular sizes for the clouds and small pathlengths, which

imply a sheet-like geometry. Thus, it appears likely that the observed lines may not be associated with the cold molecular clouds in the ISM.

The warm gas models with $T_e > 20$ K were able to explain the observed data towards several of the positions in the inner Galaxy if the cloud size was assumed to be either $4°$ or $2°$. Large cloud sizes ($\sim 25°$) were ruled out. For a cloud size of $4°$, the probable physical parameters of the lineforming region that explain the data are $T_e = 80 - 100$ K, $n_e = 0.003 - 0.01$ cm^{-3} and pathlengths of $\sim 0.1 - 2$ kpc for $T_{R100} = 2500$ K & 1250 K. On the other hand, if the cloud size is $2°$, then the probable physical parameters are $T_e = 150 - 250$ K, $n_e = 0.005 - 0.007$ cm^{-3} and pathlengths are $\sim 0.1 - 2.5$ kpc for both the radiation temperatures. The fitted parameters of the models imply pressure equilibrium with the ISM. Also, the pathlengths predicted by these models can explain the observed line widths in terms of Galactic rotation. However, we were not able to find warm models that fitted the data at all the positions, probably due to the unknown cloud size.

From our study, it appears that the low frequency carbon recombination lines are likely to arise in the neutral atomic (HI) gas in the Galaxy. However, the lack of good correlation between high HI optical depth and the detectability of carbon recombination line suggests that only a subset of the neutral clouds give rise to these lines. With the existing instruments, carbon recombination lines seem to be detectable with typical line-to-continuum ratios of a few times 10^{-4} to 10^{-3} in the inner Galaxy ($l < 20°$) as the observations by EMA95 near 76 MHz and our observations near 34.5 MHz have shown. However, the lines are not so easily-detectable in the outer Galaxy (galactocentric distances > 8 kpc). Higher sensitivity observations are required to check the existence of weaker lines which may have escaped detection. It appears probable that the ionized carbon seen in recombination lines arise at various depths within the photodissociation regions (PDR) described by Hollenbach et al (1991) which contain both atomic and molecular hydrogen and encompass a wide range of physical parameters.

Finally, in this thesis, we also studied the structure and physical properties of the partially ionized gas adjacent to the well-known classical HII region W3A. High angular resolution ($\sim 10''$), high-sensitivity images of W3A were obtained in C168α & H168α lines using the VLA. The H168α line is found to consist of a broad (> 20 kms^{-1}) and a narrow (< 10 kms^{-1}) component. While the broad line is attributable to the fully ionized HII region, the narrow line arises in the partially ionized medium (PIM) surrounding the HII region. The intense carbon and narrow hydrogen line emission is a result of stimulated emission by the background thermal region. We find from a comparison of the narrow H168α and C168α distributions across the continuum

source that the two line-forming regions, although sharing some overlap, are not entirely coextensive. The C II structure also bears some similarity with that of H_2CO which is a tracer of H_2 gas in front of the H II region. Unlike the narrow hydrogen line which arises in a thin partially ionized medium (PIM) immediately adjacent to the H II region, the C168α lines arise both in the PIM and the photodissociation region (PDR) which extends beyond the PIM. The longer pathlengths that we obtain from modelling the C II region using the observed intensities of C168α lines supports this hypothesis. If the PIM and C II regions were assumed to be coexistent, then we obtain a temperature of $\sim$ 420 K for these regions. The electron density in the PIM can range from 5 to 50 cm^{-3} whereas in the C II region the density range is 5 to 30 cm^{-3}. In addition to the observed line emission, the models were constrained by the observed' molecular densities in the adjoining molecular clouds and the theoretical size of a photodissociated region around a hot star.

The distribution of the broad hydrogen line over W3A resembles the structure of the continuum source. F'rom the peak continuum emission at 1.4 GHz and 8.3 GHz, the electron temperature of the hot ionized gas was calculated to be $\sim$ 8700 K which is in good agreement with the values obtained from observations at higher frequencies. Assuming a homogeneous spherical distribution of electrons in W3A, we derived an average electron density $n_{e,rms}$ of 2200 cm^{-3} from the flux density of W3A at 8.3 GHz. The true electron density $n_{e,true}$ in W3A, calculated from a pressure-broadened H171η line, is 2 x 10^4 cm^{-3}. F'rom these two estimates of electron densities, we constrain the filling factor $(n_{e,rms}/n_{e,true})^2$ of the H II region to be $\geq$ 0.01.

In summary, we have presented in this thesis an extensive observational study of low-frequency carbon recombination lines from the partially ionized gas associated with a widely distributed component of the interstellar medium. In addition, we have also presented a limited study of carbon and hydrogen recombination lines at a higher frequency from the partially ionized medium adjacent to a well-known H II region.

7.1 Suggestions for Future Work

This relatively young field of low-frequency carbon recombination lines needs to be further investigated. Currently, the detectability of the low-frequency lines seems to be limited to line-to-continuum ratios of a few times 10^{-4}. The limitation is due both to poor resolution of the telescopes which results in beam dilution and not enough integration time. A large filled-aperture radio telescope operating at frequencies below 100 MHz and ability to observe a large number of transitions simultaneously can give

a substantial increase in sensitivity. Such high-sensitivity single-aperture observations of carbon recombination lines in the inner Galactic plane at a range of frequencies with similar angular resolutions will prove to be very useful in further constraining the probable physical parameters of these regions. Interferometric observations with high angular resolutions and sensitivities will help in understanding the fine structure of ionized carbon in the inner Galaxy. The Giant Metre-wave Radio Telescope (GMRT) near Pune, which will be going into full operation shortly, would be a valuable instrument for these studies. Observations of several directions towards which only HI absorption or only ^{12}CO emission has been observed, will be useful in confirming the preliminary conclusion that ionized carbon in the Galaxy is associated with the cold atomic gas. High sensitivity observations of the outer Galaxy (Galactocentric distances > 8 kpc) would help in determining whether the low-frequency carbon recombination lines is a widespread phenomenon or more confined to the inner Galaxy. Presently, it appears that the high rate of detection in the inner Galaxy may be due to the strong non-thermal background in that region.

On the theoretical front it is necessary to increase our understanding of the effects of the environment on the population of high Rydberg states. Although a beginning has been made in the work of Gulyaev & Nefedov (1989) and the application of it to the direction of Cas A by Payne, Anantharamaiah & Erickson (1994), there are still many unanswered questions. The inclusion of such effects have so far not led to better models to explain the observations.

Bibliography

Adler, D.S., Wood, D.O.S., Goss, W.M., 1996, ApJ, 471, 871.

Altenhoff, W., Mezger, P.G., Wendker, H. Westerhout, G., 1960, Veroff. Sternwarte, Bonn, No. 59, 48.

Altenhoff, W.J., Downes, D., Pauls, T., Schraml, J., 1979, A&AS, 35, 23.

Anantharamaiah, K.R., PhD thesis, 1984, Bangalore University.

Anantharamaiah, K.R., 1985, J.A.A. 6, 177.

Anantharamaiah, K.R., 1986, J.A.A. 7, 131.

Anantharamaiah, K.R. & Bhattacharya, D., 1986, JAA, 7, 141.

Anantharamaiah, K.R. & Goss, W.M., 1990, in Radio Recombination Line: 25 years of investigation Ed: Gordon, M.A. & Sorochenko, R.L., ASSP, (Kluwer, Dordrecht), p 267.

Anantharamaiah, K.R. & Goss, W.M., 1996, ApJ, 466, L13.

Anantharamaiah, K.R., Goss, W.M., P.E.Dewdney, 1990, in Radio Recombination Lines: 25 Years of Investigation Ed : M.A.Gordon & R.L.Sorochenko, ASSL, (Kluwer, Dordrecht), p 123.

Anantharamaiah, K.R., Payne, H.E., Bhattacharya, D., 1990, in Radio Recombination Line: 25 years of investigation Ed: Gordon, M.A. & Sorochenko, R.L., ASSL, (Kluwer, Dordrecht), p 259.

Anantharamaiah, K.R., Payne, H.E., & Erickson, W.C., 1988, MNRAS, 235, 151.

Anantharamaiah, K.R., Erickson, W.C., Payne, H.E., Kantharia, N.G. 1994, ApJ, 430, 682.

Anantharamaiah, K.R., Zhao, J.H., Goss, W.M., Viallefond, F., 1993, ApJ, 419, 585.

Anish Roshi,D., 1995, M.Sc. Thesis, University of Poona, Pune.

Arnal, E.M., Goss, W.M., Dickel, H.R., Forster, J.R., 1982, MNRAS, 201, 317.

Bania, T.M., 1977, ApJ, 216, 381.

Baars, J.W.M., Genzel, R., Pauliny-Toth, I.I.K., Witzel, A., 1977, A&A, 61, 99.

Bennett, C.L., & Hinshaw, G., 1993, in 'Back to the Galaxy', ed. Holt, S.S. & Verter, F. (AIP Conf. Proc. 278), p257.

Bieging, J.H., Goss, W.M., Wilcots, E.M., 1991, ApJS, 75, 999.

Blake, D.H., Crutcher, R.M., & Watson, W.D., 1980, Nature, 287, 707.

Brocklehurst, M., 1970, MNRAS, 148, 417.

Brocklehurst, M., 1971, MNRAS, 153, 471.

Brocklehurst, M. & Leeman, S., 1971, Astrophys. Lett., 9, 35.

Brocklehurst, M. & Salem, M., 1977, Computer Phys. Comm., 13,39.

Brocklehurst, M. & Seaton, M.J., 1972, MNRAS, 157, 179.

Burgess, A & Summers, H.P., 1969, ApJ, 157, 1007.

Burton, W.B., Gordon, M.A., Bania, T.M., Lockman, F.J., 1975, ApJ, 202, 30.

Burton, W.B., 1988, in Galactic and Extragalactic Radio Astronomy, Ed: Verschuur, G.I., & Kellerman, K.I., 2nd ed.; Berlin:Springer, 295.

Burton, W.B. & Gordon, M.A., 1978, A&A, 63, 7.

Clemens, D.P., Sanders, D.B., & Scoville, N.Z., 1988, ApJ, 327, 139.

Cohen 1986, ApJS, 60, 695.

Cox, D.P., & Smith, B.W., 1974, ApJ (Letters), 189, L105.

Crinklaw, G., Federman, S.R., & Joseph, C.L., 1994, ApJ, 424, 748.

Deshpande, A.A., 1987, Ph.D. thesis, Indian Institute of Technology, Bombay.

Deshpande, A.A., Shevgaonkar, R.K., Shastry, CH.V., JIETE, 35, 1989, 342.

Despois, D., & Baudry, A., 1985, A&A, 148, 83.

Diamond, P.J., Goss, W.M., Romney, J.D., Booth, R.S., Kalberla, P.M.W., Mebold, U., 1989, ApJ, 347, 302.

Dickel, H.R., Harten, R.H., Gull, T.R., 1983, A&A, 125, 320.

Dravskikh, Z.V., & Dravskikh, A.F., 1964, Astron. Tsirk., 282, 2.

Dupree, A.K., 1972, ApJ, 173, 293.

Dupree, A.K., Goldberg L., 1970, AA&AR, 8, 231.

Dwarakanath, K.S., 1989, Ph.D. thesis, Indian Institute of Science, Bangalore.

Erickson, W.C., McConnell, D., Anantharamaiah, K.R., 1995, ApJ, 454, 125. (EMA85)

Ershov, A.A., Ilyasov, Yu.P., Lekht, E.E., Smirnov, G.T. Solodkov, V.T., & Sorochenko, R.L. 1984, Sov. Astron. Lett., 10, 348.

Ershov, A.A., Lekht, E.E., Smirnov, G.T., Sorochenko, R.L., 1987, Sov. Astron. Lett., 13, 8.

Field, G.B., Goldsmith, D.W., Habing, H.J., 1969, ApJ (Letter), 155, L149.

Frail, D.A., Weisberg, J.M., Cordes, J.M., Mathers, C., 1994, ApJ, 436, 144.

Garwood, R.W., & Dickey, J.M., 1989, ApJ, 338, 841.

Griem, H.R., 1967, ApJ, 148, 547.

Goldberg, L., 1966, ApJ, 144, 1225.

Goldberg, L., & Dupree, A. K., Nature, 1967, 215, 41.

Golynkin, A.A. & Konovalenko, A.A., 1990, in Radio Recombination Line: 25 years of investigation Ed: Gordon, M.A. & Sorochenko, R.L., ASSL, (Kluwer, Dordrecht), p 209.

Gordon, M. A., in Galactic and Extragalactic Radio Astronomy, Ed: Verschuur, G.I., & Kellerman, K.I., (2nd ed.; Berlin:Springer), p 37.

Gordon, M.A., 1989, ApJ, 337, 782.

Gordon, M.A., & Meeks, M.L., 1967, ApJ, 149, L21.

Gottesman, S.T., & Gordon, M.A., 1970, ApJ (Letters), 162, L93.

Gulyaev, S.A., Nefedov, S.A. 1989, Astron. Nach., 310, 403.

Hart, L. & Pedlar, A. 1976, MNRAS, 176, 547.

Hart, L. & Pedlar, A. 1980, MNRAS, 193, 781.

Haslam, C.G.T., Stoffel, H., Salter, C.J., Wilson, W.E., 1982, A&AS, 47, 1.

Hayes, M.A., & Nussbaumer, H., 1984, A&A, 134, 193.

Heiles, C., 1994, ApJ, 436, 720.

Heiles, C., Reach, W.T., Koo, Bon-Chul, 1996, ApJ, 466, 191.

Henkel, C., Walmsley, C.M., Wilson, T.L., 1980, A&A, 82, 41.

Hoang-Binh, D., Encrenaz, P. & Linke, R.A., 1985,A & A, 146, L19.

Hoglund, B., & Mezger, P.G., 1965, Science, 150, 339.

Hollenbach, D. J., 1990, in 'The Evolution of the Interstellar Medium' Ed: Blitz, L., ASP Conf. Ser., Vol 12, p 167.

Hollenbach, D. J., Takahashi T., Tielens, A.G.G.M., 1991, ApJ, 377, 192. (HTT91)

Howe, J.E., Jaffe, D.T., Genzel, R., Stacey, G.J., 1991, ApJ, 373, 158.

Howe, J.E., Jaffe, D.T., Zhou, S., 1995, ASP, Airborne Astronomy Symposium on the Galactic Ecosystem: From Gas to Stars to Dust, Vol 73, p 91-92.

Hummer, D.G., & Mihalas, D. 1988, ApJ, 331, 794.

Martin-Pintado, J., Bachiller, R., Thum, C., & Walmsley, W.M., 1989, A&A, 215, L13.

Jackson, P.D. & Kerr, F.J., 1971, ApJ, 168, 29.

Jaffe, D.T., & Wilson, T.L., 1981, ApJ, 246, 113.

Jenkins, E.B., Jura, M., Loewenstein, M., 1983, ApJ, 270, 88.

Jenkins, E.B., 1987, in Interstellar Processes, ed. D.J.Hollenbach & H.A.Thronson (Dordrecht:Reidel), p 533.

Kardeshev, N.S., 1959, Astron. Zh. 36, 838.

Kazes, I.,, & Crovisier, J., 1981, A & A, 101, 401.

Konovalenko, A.A., 1984, Sov Astr. Lett., 10, 912.

Konovalenko, A.A., 1990, in Radio Recombination Lines: 25 Years of Investigation, Ed : M.A.Gordon & R.L.Sorochenko, ASSL, (Dordrecht,Kluwer), p 175.

Konovalenko, A.A., & Sodin, L.G., 1979, Sov. Astron. Lett., 5, 355.

Konovalenko, A.A., & Sodin, L.G., 1980, Nature, 283, 360.

Konovalenko, A.A., Sodin, L.G., 1981, Nature, 294, 135.

Kulkarni, S. & Heiles, C., 1988 in Galactic and Extragalactic Radio Astronomy, ed: Verschuur, G.H., Kellerman, K.I., Springer-Verlag, Berlin, 95.

Lockman, F. J., 1976, ApJ, 209, 429.

Lockman, F. J., 1984, ApJ, 283, 90.

McKee, C. & Ostriker, J., 1977. ApJ, 196, 565.

Menzel, D.H., 1937, ApJ, 85, 330.

Mezger, P.G., & Henderson, A.P., 1967, ApJ, 147, 471.

Onello, J. & Phillips, J.A., 1995, ApJ, 448, 727.

Oster, L., 1961, Rev. Mod. Phys., 33, 525.

Osterbrock, D.E. in Astrophysics of Gaseous Nebulae & Active Galactic Nuclei, University Science Books, California, 1989, p 165.

Palmer P., Zuckerman, B., Penfield, H., Lilley A.E., Mezger, P.G., 1967, Nature, 215, 40.

Pankonin, V., Walmsley, C.M., Wilson, T.L., Thomasson, P., 1977, A. & A. 57, 341.

Pankonin, V., Thomasson, P., Barsuhn, J., 1977a, A&A, 54, 335.

Payne, H.E., Anantharamaiah, K.R., Erickson, W.C., 1989, ApJ, 341, 890. (PAE89)

Payne, H.E., Anantharamaiah, K.R., Erickson, W.C., 1994, ApJ, 430, 690. (PAE94)

Payne H.E., Salpeter E.E., Terzian Y., 1984, AJ, 89, 668.

Peach, G., 1972, Astrophys. Lett., 10, 129.

Pedlar, A., Davies, R.D., Hart, L., Shaver, P.A., 1978, MNRAS, 182, 473.

Petuchowski, S.J., & Bennett. C.L., 1993, ApJ, 405, 591.

Ponomarev, V.O., & Sorochenko, R.L., 1992, Sov. Astron. Lett., 18, 215.

Radhakrishnan, V., Goss, W.M., Murray, J.D., Brooks, J.W., 1972, ApJS , 24, 1.

Radhakrishnan, V., Goss, W.M., Murray, J.D., Brooks, J.W., 1972, ApJS, 24, 49.

Ravindra, D.K., 1983, Ph.D. Thesis, Indian Institute of Science, Bangalore.

Reich, W., Fuerst, E., Reich, P., Reif, K., 1990, A&AS, 85, 633.

Reynolds, R.J., 1984, ApJ, 282, 191.

Richardson, K.J., White, G.J., Phillips, J.P., Avery, L.W., 1986, MNRAS, 219, 167.

Rodriguez, L.F. & Chaisson, E.J. 1979, ApJ, 228, 734.

Roelfsema, P.R. & Goss, W.M., 1992, The A&AR, 4, 161.

Roelfsema, P.R., Goss, W.M., Mallick, D.C.V., 1992, ApJ, 394, 188.

Roelfsema, P.R. & Goss, W.M., & Wilson, T.L., 1987, A&A, 174, 232.

Roelfsema, P.R., 1987, Ph.D thesis, University of Groningen, The Netherlands.

Roger, R.S., & Dewdney, P.E., 1992, ApJ, 385, 536.

Anish Roshi, D. & Anantharamaiah, K.R., 1997, MNRAS (in press).

Salem, M. & Brocklehurst, M., 1979, ApJS, 39, 633.

Scoville, N.Z., 1990, in The Evolution of the ISM, Ed: Blitz, L., ASP Conf. Ser., Vol 12, p49.

Scoville, N.Z., & Solomon, P.M., 1975, ApJ, 199, L10.

Scaquist, E.R., & Bell, M.B.,1977, A&A, 60, L1.

Shaver, P.A., 1975, Pramana, 5, 1.

Shaver, P.A., 1976, A&A, 46, 127.

Shaver, P.A., 1980, A & A, 91, 279.

Shaver, P.A., Churchwell, E., Rots, A.H., 1977, A&A,55,435.

Shaver, P.A., Pedlar, A., Davies, R.D., 1976, MNRAS, 177, 45.

Shibai et al, 1991, ApJ, 374, 522.

Shibai Hiroshi et al., 1996, PASJ, 48, L127.

Smirnov, G.T., Kitaev, V.V., Sorochenko, R.L., & Schegolev, A.F., 1996, *Annual Session of Sci. Council of Astrocosmical Center of P. N. Lebedev Phys. Inst.*, Puschino 1995, Collection of Reports, 3.

Sorochenko, R.L., 1996, A&A Trans, 11, 199.

Sorochcnko, R.L., & Borozich, E.V., 1964, Rep. of the Sov. Acad. of Science, 162, 3. 603.

Sorochenko, R.L. & Smirnov, G.T., 1993, Sov. Astron. Lett., 19, 2.

Sorochenko, R.L. & Smirnov, G.T., 1990, in Radio Recombination Line: 25 years of investigation Ed: Gordon, M.A. & Sorochenko, R.L., ASSP, (Kluwer, Dordrecht), p 189.

Sorochenko, R.L. & Walmsley, C. M., 1991, A&A Trans, 1, 31.

Sorochenko, R.L., Smirnov, G.T., Rydbeck, G., 1988, A&A, 198, 233.

Sridharan, T.K., 1992, Ph.D. Thesis, Indian Institute of Science, Bangalore.

Subrahmanyan, R., Ph.D. Thesis, 1989.

Subrahmanyan, R., & Goss, W.M., 1996, MNRAS, 281, 239.

Swarup, G., Sarma, N.V.G., Joshi, M.N., Kapahi, V.K., Bagri, D.S., Damle, S.H., Ananthakrishnan, S., Balasubramanian, V., Bahve, S.S., Sinha, R.P., 1971, Nature, Phys. Science (Lond), 230, 185.

Tielens, A.G.G.M., & Hollenbach, D.J., 1985, ApJ, 291, 722.

Udayshankar, N., 1986, Ph.D. Thesis, Bangalore University, Bangalore.

van der Hulst, J.M., Terlouw, J.P., Begeman, K, Zwitser, W & Roelfsema, P.R., on GIPSY in Astronomical Data Analysis Software and Systems I, eds: Worall, D.M., Biemesderfer, C., & Barnes, J., ASP Conf. Series no. 25, p.131, 1992.

van der Werf & Goss, W.M., 1990, A&A, 238, 296.

van Gorkom, J.H., 1980, Ph.D thesis, University of Groningen, The Netherlands.

Walmsley, C.M., Watson, W.D. 1982, ApJ, 260, 317.

Watson, W.D., Western, L.R., Christensen, R.B., 1980, ApJ, 240, 956.

Zhao, J.H., Anantharamaiah, K.R., Goss, W.M., Viallefond, F., 1996, ApJ, 472, 54.